REPUBLIC OF CAMEROON

REPUBLIQUE DU CAMEROUN

MINISTRY OF HIGHER EDUCATION

MINISTERE DE L'ENSEIGNEMENT SUPERIEUR

Ecole Nationale Supérieure des Travaux Publics

UNIVERSITÀ DEGLI STUDI DI PADOVA

DEPARTMENT OF CIVIL ENGINEERING

DEPARTEMENT DE GENIE CIVIL

DEPARTMENT OF CIVIL, ARCHITECTURAL AND ENVIRONMENTAL ENGINEERING

COLLAPSE OF BRIDGES FROM THE TWENTIETH CENTURY TO TODAY: CAUSES AND IMPROVEMENTS

CASE STUDY: BRIDGE OVER THE MAYO LIMANI IN THE FAR NORTH REGION OF CAMEROON

A thesis submitted in partial fulfilment of the requirements for the degree of Master of Engineering (MEng) in Civil Engineering

Curriculum: **Structural Engineering**

Presented by:

BONYARE INROMBE Barnabas

Student Matricula number: **16TP21217**

Supervised by:

Prof. Carmelo MAJORANA

Co-supervised by:

Dr. Eng. Guillaume Hervé POH'SIE

Dr. Eng. Emanuele MAJORANA

Academic year: 2020/2021

REPUBLIC OF CAMEROON

REPUBLIQUE DU CAMEROUN

MINISTRY OF HIGHER EDUCATION

MINISTERE DE L'ENSEIGNEMENT SUPERIEUR

Ecole Nationale Supérieure des Travaux Publics

UNIVERSITÀ DEGLI STUDI DI PADOVA

DEPARTMENT OF CIVIL ENGINEERING

DEPARTEMENT DE GENIE CIVIL

DEPARTMENT OF CIVIL, ARCHITECTURAL AND ENVIRONMENTAL ENGINEERING

COLLAPSE OF BRIDGES FROM THE TWENTIETH CENTURY TO TODAY: CAUSES AND IMPROVEMENTS

CASE STUDY: BRIDGE OVER THE MAYO LIMANI IN THE FAR NORTH REGION OF CAMEROON

A thesis submitted in partial fulfilment of the requirements for the degree of Master of Engineering (MEng) in Civil Engineering

Curriculum: **Structural Engineering**

Presented by:

BONYARE INROMBE Barnabas

Student Matricula number: **16TP21217**

Supervised by:

Prof. Carmelo MAJORANA

Co-supervised by:

Dr. Eng. Guillaume Hervé POH'SIE

Dr. Eng. Emanuele MAJORANA

Academic year: 2020/2021

DEDICATION

To my family

Especially to my beloved parents

ACKNOWLEDGEMENTS

This work would not have been completed without the combined efforts of individuals who contributed directly and/or indirectly to its realization. I wish to express my sincere thanks and gratitude to:

- The **President** of the jury for the honour of accepting to preside this jury;
- The **Examiner** of this jury for accepting to bring his criticisms and observations to ameliorate this work ;
- **Prof. NKENG George ELAMBO** and **Prof. Eng. Carmelo MAJORANA** for all their academic and administrative support during these five years spent at ENSTP in the MEng program in partnership with University of Padua in Italy ;
- The vice-director of ENSTP**, Dr M. BWEMBA Charles Loic** for his perpetual help and advices during the so journey in this school ;
- **Prof. Michel MBESSA**, the head of department of Civil Engineering for his tutoring and valuable advices ;
- My supervisors **Prof. Eng Carmelo MAJORANA**, **Dr. Eng. Guillaume Hervé POH'SIE** and **Dr. Eng. Emanuele MAJORANA** for all the guidance and advices they provide me with, during this thesis work;
- All the **teaching staff** of **ENSTP** and **University of Padua** for their good quality teaching and the motivation they developed in us to continue the studies ;
- My parents, **INROMBE Jermias** and **FANTA**, for the education and financial support during all these years;
- The whole **INROMBE** families for the moral, social and financial support;
- All my classmates and my friends of the **7th batch** of Master's in Engineering (MEng) of The National Advanced School of Public Works who were a source of motivation and tenacity;
- My friends and all those who helped me, let them have my profound gratitude.

LIST OF ABBREVIATIONS AND SYMBOLS

ABBREVIATIONS

AASHTO	American Association of State Highway and Officials
BIR	Bataillon d'Intervention Rapide
DOA	Direction des Ouvrages d'Art
EC	Eurocode
EN	European Norm
HMTD	Hexamethlene Triperoxide Diamine
RC	Reinforce Concrete
SHM	Structural Health Monitoring
SLS	Serviceability Limit State
TATP	Triacetone - Triperoxide
TNT	Trinitrotolueme
TS	Tandem Load
ULS	Ultimate Limit State
USA	United States of America
WIM	Weigh In Motion

SYMBOLS

$\dot{\mathbf{u}}_{(t)}$	System velocity
$\mathbf{A'_s}$	Area of upper steel reinforcement section
$\mathbf{A_C}$	Slab section area
$\mathbf{A_d}$	Accidental load
$\mathbf{A_{s,min}}$	Minimum steel reinforcement section area
$\mathbf{A_{s,provided}}$	Effective area of steel reinforcement
$\mathbf{A_s}$	Area of the lower steel reinforcement section
$\mathbf{A_s, max}$	Maximum steel reinforcement section area
$\mathbf{A_{sw}}$	Cross sectional area of the shear reinforcement
$\mathbf{E_c}$	Elastic modulus of concrete
$\mathbf{E_{cm}}$	Concrete elastic modulus

$\mathbf{E_s}$	Elastic modulus of steel
$\mathbf{G_{k,j}}$	Permanent loads
$\mathbf{M_{Ed}}$	Soliciting bending moment
$\mathbf{M_{Rd}}$	Resisting moment
$\mathbf{N_{Ed}}$	Design axial value
$\mathbf{N_{Ed}}$	Design axial compressive force
$\mathbf{N_{beam}}$	Shrinkage load per beam
$\mathbf{N_{c,r\infty}}$	Shrinkage load
$\mathbf{Q_{k,i}}$	Variable loads
$\mathbf{TS_k}$	Tandem load
$\mathbf{T_k}$	Temperature load
$\mathbf{UDL_k}$	Uniform distributed load
$\mathbf{V_{Ed}}$	Design shear value
$\mathbf{V_{Ed}}$	Design shear value
$\mathbf{V_{Rd}}$	Resisting shear
$\mathbf{V_{rdc}}$	Shear capacity of concrete
$\mathbf{c_{min,b}}$	Minimum cover due to bond requirement
$\mathbf{c_{min,dur}}$	Minimum cover due to environmental conditions
$\mathbf{c_{min}}$	Minimum concrete cover
$\mathbf{f_{cd}}$	Design compressive strength of concrete
$\mathbf{f_{ctm}}$	Tensile strength of the concrete
$\mathbf{f_{yd}}$	Design yielding strength of steel
$\mathbf{f_{yk}}$	Characteristic yield strength of steel
$\mathbf{f_{ywd}}$	Design yield strength of the shear reinforcement
$\mathbf{i_s}$	Positive impulse
$\mathbf{q * f_k}$	Traffic load on footways
$\mathbf{r_m}$	Moment ratio
$\boldsymbol{K_s}$	Modulus of subgrade reaction
$\boldsymbol{l_0}$	Effective length of the element
$\boldsymbol{\alpha_{cw}}$	Coefficient of interaction between compressive stresses
$\boldsymbol{\alpha_{0ik}}$	Values of adjustment factors
$\boldsymbol{\gamma_{G,j}}$	Partial factors of permanent loads
$\boldsymbol{\gamma_{Q,i}}$	Partial factors of variable loads

$\varepsilon_{ca}(\infty)$	Autogenous shrinkage
$\varepsilon_{cd}(\infty)$	Dry shrinkage at infinite
λ_{lim}	Limit value of slenderness
ρ_1	Shear reinforcement ratio
σ_c	Stress in concrete
σ_s	Stress in steel reinforcement
ϕ_{lmin}	Minimum diameter of the longitudinal bars
[C]	Damping matrix
[K]	Stiffness matrix
[M]	Mass matrix
A	Area of the cross section
Ac	Area of the concrete cross section
b	Width of the element
cc	Concrete cover
d	Effective depth of the section
$E_{c,eff}$	Reduced modulus of elasticity for concrete
i	Gyration radius of the uncracked concrete section
J	Moment of inertia of the section
l	Span length of the beam
p(t)	Dynamic load
Po	Ambient pressure
P_{so}	Peak over-pressure
P_{so}^-	Minimum pressure
R	Standoff distance
s	Stirrup spacing
t_A	Arrival time of blast
T_{beam}	Temperature load per beam
t_o	Positive phase duration
t_o^-	Negative phase duration
u(t)	System displacement
ü(t)	System acceleration
W	Explosive weight
Z	Scaled distance

z	Inner lever arm
v1	Reduction coefficient of shear crack
y	Neutral axis position
α	Angle between shear reinforcement and axis of design element
ε	Thermal coefficient
λ	Slenderness
χ	Reduction factor
ψ	Multipliers for the characteristic values of variable loads

ABSTRACT

The main objective of this work was to evaluate the partial collapse of a concrete bridge, caused by the instability of a pier under the effect of explosive loads. The case study for this thesis was a reinforced concrete girder bridge built at Limani in the Far North region of Cameroon. To achieve this objective, a literature review was first carried out in order to gain an insight into the general causes of bridges collapse, the mechanisms of explosion-induced bridges collapse in particular and the definition of explosive loads. The former was ensued by a methodology where details for a static analysis procedure were enumerated. They included the evaluation of the static loads acting on the bridge and the various verification conditions for each section according to the Eurocode (0, 1, 2 and 7) standards. Thereafter, the pressures induced by the explosion were computed with the aid of an excel spreadsheet. After that, the explosion was taken into account on the deck, by applying an explosive mass of TNT (0.1 kg) to the second pier (P2) of the bridge and the influence of its parameters on the local response of the structural components was determined. Subsequently, a non-linear dynamic analysis was carried out with the MIDAS/civil 2022 software. The results obtained limpidly indicated that the stresses did not exceed the capacity of the structural elements, but the explosion caused an instability of the foundations due to the high loads, which led to the partial collapse of the first three bridge decks with uncoupling of the second pile. Finally, solutions such as the straightening beam, increased foundation dimensions and raft foundations were designed to overcome the identified instability problem.

Keywords: collapse of bridges, blast, time-history analysis, instability, improvements.

RESUME

L'objectif principal de ce travail était d'évaluer l'effondrement partiel d'un pont en béton, causé par l'instabilité d'une pile sous l'effet des charges explosives. Le cas d'étude pour ce mémoire était un pont à poutres en béton armé construit à Limani dans la région de l'Extrême-Nord au Cameroun. Pour atteindre cet objectif, une revue de la littérature a tout d'abord été effectuée afin d'avoir un aperçu des causes en générales de l'effondrement de ponts, des mécanismes d'effondrement de ponts provoqués une explosion en particulier et de la définition des charges explosives. La partie précédente a été suivie d'une méthodologie où les détails d'une procédure d'analyse statique ont été énumérés. Ils comprennent l'évaluation des charges statiques agissant sur le pont et les différentes conditions de vérification pour chaque section selon les normes Eurocode (0, 1, 2 et 7). Ensuite, les pressions induites par l'explosion ont été calculées à l'aide d'un tableur Excel. Après quoi, l'explosion a été prise en compte sur le pont, en appliquant une masse explosive de TNT (0,1 kg) sur la deuxième pile (P2) du pont et l'influence de ses paramètres sur la réponse locale des composants structurels a été déterminée. Par la suite, une analyse dynamique non linéaire a été réalisée avec le logiciel MIDAS/civil 2022. Les résultats obtenus indiquent clairement que les contraintes n'ont pas dépassé la capacité des éléments structurels, mais l'explosion a provoqué une instabilité des fondations due aux fortes sollicitations, ce qui a conduit à l'effondrement partiel des trois premiers tabliers du pont avec désolidarisation de la deuxième pile. Enfin, des solutions telles que la poutre de redressement, l'augmentation des dimensions des fondations et les fondations sur radier ont été conçues pour surmonter le problème d'instabilité identifié.

Mots clés : Effondrement des ponts, explosion, analyse dynamique non-linéaire, instabilité, améliorations.

LIST OF FIGURES

LIST OF TABLES

TABLE OF CONTENTS

GENERAL INTRODUCTION

Bridge collapses can be tragic events, leading to loss of life and serious property damage. That is why bridge engineers, designers and builders must always take their jobs very seriously. The best way for them to prevent these accidents is to first understand the factors associated with bridge collapses. Understanding the causes of bridge collapses can lead to major changes in the design, construction and safety of future building projects. In recent years, with the increase in accidental and violent blast events through the world, the importance of protecting the public transportation infrastructure, especially bridges, from blast collapse has become increasingly significant. However, the current engineering design codes have almost no specific provisions or guidelines for blast protection of bridges.

With this in mind, structural engineers and other professionals are continuously researching and developing cost-effective methodologies in order to have a better comprehension of bridges behaviour under blast loads and also to protect lives.

The key objective of this thesis is to evaluate the partial collapse of a concrete bridge, caused by the instability of a pier under the effect of blast loads by using software MIDAS/civil 2022.

In order to achieve this objective, the study is divided in three chapters. The first chapter consists of a literature review on the causes of bridge collapse, the mechanisms of bridge collapse due to blast, the consequences of bridge failures as well as the definition of blast load. The second chapter deals with the methodology. Here, the approach used for the determination of the loads and the static checks, the dynamic analysis procedure as well as the method used to model the blast load acting on the bridge for a numerical analysis, will be presented. In the last chapter which is the presentation of the results and their interpretations, the study case will be detailed first. Secondly, static analysis and corresponding verifications will follow. The third point concerns the effects of blast loads on bridge. Finally, some possible solution are highlighted to improve to reduce the stability of footing will be evaluated.

CHAPTER 1: LITERATURE REVIEW

Introduction

The objective of this chapter is to present a literature review on causes of bridge collapse and mechanism of bridge collapse due to blast. Furthermore, the consequences of bridge failures are highlighted. Finally, a review of available literature on blast concept and its related parameters will be made.

1.1. Causes of bridge collapse

The failure during the construction, the failure during the service, the natural factor of collapse and the human factor of collapse are discussed in this part.

1.1.1. Failure during the construction

Construction or erection of a bridge structure is as crucial as design of bridge. Lack of expertise and experience of site engineers can be most common reasons apart from instability issues during construction. In steel bridges, buckling is the most common cause of collapse during erection if the actual lateral supports are weaker or does not reflect the one assumed in the design. Insufficient bearing capacity of soil due to improper ground treatment can be a reason.

Another important cause of failure during construction is the failure of material, due to manufacturing defects or over-stressing beyond limits. Improper erection causing tilts foundation if not addressed leads to collapse. Irresponsibility, ignorance and indifference are primary caused of failure of bridges during construction.

1.1.2. Failure during the service

During service, the causes of failure of bridges (the sample size is 2010) are shown in figure 1.1. Various causes of failure of bridges are overloads, deterioration of material including ageing, natural disasters, design as well as construction aspects and human-made disasters, and the values are provided in table 1.1. The dominant cause is the natural disasters of the order of 80.30%. Another dominating cause of failures is the deterioration of the material (10.10%) followed by the design and construction (4.13%). The overloading is the cause of 3.28%, and Human-Made disasters are 2.19% of all the failures of bridges in India (Garg et al., 2020).

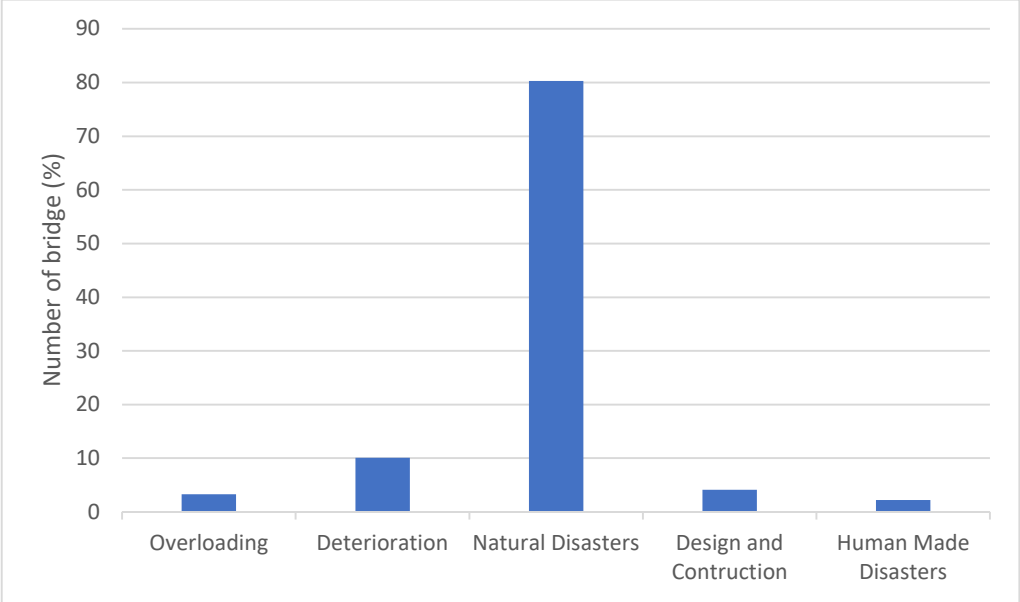

Figure 1.1. Causes of bridge failures during service data from (Garg et al., 2020).

Table 1.1. Causes of bridge failures during service from (Garg et al., 2020).

Cause of Failure	**Number of bridges (percentage)**		
Overloading			66 (3.28%)
Deterioration			203 (10.10%)
	Concrete	47	
	Steel	15	
	Masonry	15	
	Timber	5	
	Dilapidated & demolished	103	
Natural disasters			1614 (80.30%)
	Flood	1029	
	Scouring	14	
	Earthquake	540	
	Storm	12	
	Landslide	17	
	Snow	2	
Design and construction			83 (4.13%)
Human-made disasters			44 (2.19%)
	Accident	19	

	Blast	25	
	Total		2010 (100%)

1.1.3. Natural factor

Natural disasters which include hydraulic-induced (flood and scour), earthquake (and tsunami), storm (and cyclone), landslide and due to snow or avalanche are significant reasons for the failure of the order of 80.30% (Garg et al., 2020). The cause of disasters of bridge failures in the USA is reported as 59.25% (Wardhana & Hadipriono, 2003), 60.20% (Cook & Barr, 2017) and 54.46% (Taricska, 2014). Relatively low value implies that the bridges in the USA have been designed with greater resilience than in India against disaster events. Comparison of causes of failures available from various researchers is made and presented in table 1.2.

Table 1.2. Comparison of sample size and causes of bridge failures during.

Parameter of study	Bridges in India	Bridges in the USA (Wardhana & Hadipriono, 2003)	Bridges in the USA (Cook & Barr, 2017)	Bridges in the USA (Lee et al., 2013, MCEER)	Bridges in the USA (Taricska, 2014)	Bridges worldwide (Imam &	Bridges in China (Tan et al., 2020)
Sample period (years)	1977-2017	1989-2000	1987-2011	1980-2012	2000-2012	Before 2004	2009-2019
Sample size for reasons of failure (quantity)	2010	503	691	1062	314	164	298
Average age of failed bridges (years)	34.53	52.50	54.80	51.70	58.00	NA	23.60
Average annual rate of failure of bridges (years)	129	NA	128	NA	NA	NA	38
Causes of Failures (%)							
Overloading	3.28	8.75	11.29	12.71	13.06	5	12.76

Deterioration	10.10	9.54	9.55	6.69	7.64	3	Nil
Natural disaster	80.30	59.25	60.2	50.66	54.46	21	38.85
Design, construction and maintenance	4.13	3.18	2.32	11.11	4.77	35	12.06
Human-made disasters	2.19	14.91	15.63	18.17	17.52	14.00	26.23
Others	Nil	4.37	1.01	0.66	2.55	22.00	10.10
Total	100	100	100	100	100	100	100

1.1.3.1. Flood

Heavy precipitation usually leads to flooding, which may induce phenomena such as scour, erosion, river convergence, insufficient embedment depth, protection works-induced over fall or hydraulic jump, softened bedrock, sand mining, debris impact or abrasion on bridge foundations (Hon;Wang et al., 2014). One or a combination of these causes can result in dramatic reductions in the strength and stability of bridge key components and can even cause bridge failures, as shown in figure 1.2.

Figure 1.2. Bridge collapse due to flooding at Mahad over Savitri River of India (Limaye & Pujari, 2020).

The failure of bridges against floods alone in India is 51.89% (Garg et al., 2020) and is a serious cause of collapse. It is sometimes associated with uncontrolled sand mining. In the USA, the reported collapse of bridges due to floods (including scouring) is 52.88% (Wardhana &

Hadipriono, 2003), 54.85% (Cook & Barr, 2017) and 44.90% (Taricska, 2014). The variation of the failure rates in the USA got influenced by dominating disaster events occurred during the period of study. The failure of the pier or the direct dislodgement of the superstructure is the common failure mode of bridges in flood. The collapse of a pier may trigger the collapse of several superstructure spans.

1.1.3.2. Scour

Scour is a phenomenon in which the level of the riverbed becomes lower under the effect of water erosion, leading to the exposure of bridge foundations (AASHTO, 2012). With an increase in scour depth, the lateral resistance of the soil supporting the foundation is significantly reduced, thus increasing the lateral deflection of the foundation head (Choudhury & Hasnat, 2015). Furthermore, when the critical scour depth is reached, bending buckling of the foundation may occur under the combined effect of the dead load of bridge superstructures and the traffic load (Choudhury & Hasnat, 2015).

1.1.3.3. Earthquake

Earthquakes lead to vertical and horizontal ground motions that can result in the failure of bridge substructures (Lin et al., 2012). The vertical ground motion causes significant fluctuating axial forces in bridge columns or piers, which may induce outward buckling or crushing of the columns or piers (Kunnath et al., 2008) , as shown in figure 1.3. Moreover, the vertical ground motion can result in significant amplification of the bending moment at the bridge mid-span, which may lead to the bending failure of the bridge deck (Kunnath et al., 2008). Unlike the vertical ground motion, the horizontal ground motion mainly contributes to the shear failure of bridge columns or piers (Sun et al., 2012). In addition, both the vertical and horizontal ground motions may cause the liquefaction of the soil at the bridge foundations, which can greatly reduce the load-carrying capacity of the foundations and even directly lead to bridge collapse (Deng et al., 2016), as shown in figure 1.4.

Figure 1.3. Insufficient confinement of columns (Northridge, California 1994).

Figure 1.4. Liquefaction (West Grand Viaduct, Loma Prieta, 1989).

1.1.3.4. Landslide

The occurrence of a landslide is mainly due to water saturation, earthquake, or volcanic eruption, and it may result in the downward and outward movement of slope-forming materials including rock, soil, artificial fill, or a combination of these materials (Iverson, 2000). These moving slope forming materials, when hitting the bridge, will lead to severe damage or even collapse of the bridge, as shown in figure 1.5.

Figure 1.5. Collapse of a bridge due to landslide(Lin et al., 2012).

1.1.3.5. Hurricane and typhoon

Hurricanes and typhoons are tropical cyclones that refer to low pressure systems that generally form in the tropics. They travel with wind waves accompanied by storm surges, which raise the water level to an elevation that is able to strike the superstructure of bridges along the coast. Bridge decks may be knocked off the pile caps by the impulsive vertical and horizontal forces generated by the storm waves riding on high surges (Chen et al., 2009), as illustrated in figure 1.6. Moreover, after making their landfall, hurricanes usually lead to heavy rainfalls and cause a series of subsequent disasters such as flood, landside, and debris flow (Wang et al., 2014).

Figure 1.6. Bridge decks knocked off pile caps during hurricane to Biloxi Bay Bridge (Robertson et al., 2007).

1.1.3.6. Wind

Wind could induce aerostatic and aerodynamic instability problems for flexible long-span bridges. Aerostatic instability can be categorized into two types according to the modes of static instability, namely, torsional divergence and lateral-torsional buckling (Cheng et al., 2002). Aerodynamic vibration is usually caused by three different types of oscillations, namely, flutter, buffeting, and vortex-induced oscillation (Scanlan et al., 1998). Both aerostatic and aerodynamic forces may lead to large displacements and stresses that may exceed the capacity of bridge structures such as decks and cables, resulting in the collapse of bridges (Cheng et al., 2002), as shown in figure 1.7.

Figure 1.7. Collapse of the original Tacoma Narrows Bridge in 1940(Choudhury & Hasnat, 2015).

1.1.4. Human factor

In addition to the natural factors, human factors, including imperfect design and construction method, collision, vehicle overloading, fire, terrorist attack, lack of inspection and maintenance, etc., may also result in bridge collapses. These factors are discussed in the following sections.

1.1.4.1. Imperfect design and construction

In many cases, errors stemming from an imperfect design, willful use of inferior materials, or adoption of an inappropriate construction method can lead to bridge collapse in the construction phase (Mitropoulos et al., 2005). For example, the collapse of the West Gate Bridge in Australia in 1970 was due to the poor design and the inappropriate construction methods used (Biezma & Schanack, 2007a), while the failure of the Kutai-Kartanegara Bridge in Indonesia in 2011 was due to overstress in the connections that resulted from an imperfect connection design and questionable material selection (KAWAI et al., 2014). Therefore, strict process control and proper supervision can effectively reduce the probability of this type of bridge failure.

The cause of weakness in the design and construction practices amounts to 4.13%. In the USA, the failures due to design and construction practices are of the order of 3.18% (Wardhana & Hadipriono, 2003), 2.32% (Cook & Barr, 2017), 11.11% (Lee et al., 2013) and 4.77% (Taricska, 2014). In general, USA is no more vulnerable to these mistakes. There is a general

feeling that employment of relatively more sophisticated construction technologies coupled with appropriate design and maintenance practices are prevailing in the USA and also in China (Xu et al., 2016). Imam and Chryssanthopoulos (2012) have observed some 35.00% of failures due to design and construction issues for metallic bridges. The design and construction issues for metallic bridges involve design errors and human errors. Further, they highlighted the lack of understanding about the behavior of the metallic bridges (termed as limited knowledge) which is an additional cause of failure of such bridges of the order of 22.00%. The current advancements in analytical methods, as well as experimental facilities and better construction practices, should otherwise reduce the influence of design and construction issues for the failure of bridges during the service stage

1.1.4.2. Collision

Accidental collisions between vehicles and bridge superstructures and between vessels and bridge piers or columns can be unpredictable, as shown in figure 1.8. During the collision, very large lateral forces are transmitted to the impacted bridge structures. This large impact force, acting on a relative small contact area, can cause very high local pressure and therefore local damage to bridge components. Furthermore, as the bridge absorbs the dynamic collision energy, significant inertial forces and vibrations will be developed. Collision forces can, therefore, lead to severe damage to bridge components or even collapse of the bridge (Limaye & Pujari, 2020).

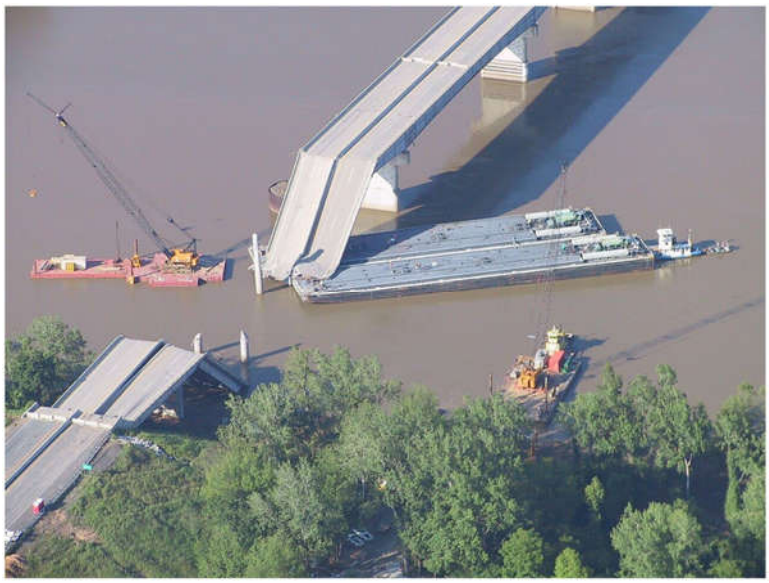

Figure 1.8. Collapse of a bridge due to vessel impact(Choudhury & Hasnat, 2015).

1.1.4.3. Vehicle overloading

Due to the increasing competition in the transportation market, vehicle overloading has become more and more common and has raised serious concerns around the world. Truck overloading usually causes fatigue problems in bridge components and can shorten the service life of bridges (Biezma & Schanack, 2007b). In some extreme cases, the weight of the overloaded trucks may even exceed the load-carrying capacity of the bridge and directly cause bridge collapse (Choudhury & Hasnat, 2015), as shown in figure 1.9.

Figure 1.9. Bridge collapse due to an overloaded truck(Garg et al., 2020).

The overloading of vehicles may contribute to accelerated fatigue damage (Lin et al., 2012). Accordingly, Colombia has incorporated the enhancement of the design load by 15% to make safe the bridges against possible overloading by vehicles. (Xu et al., 2016) have reported the failure of bridges due to overloading in China of the order of 50% of all failures during service. In another study, (Tan et al., 2020) have observed 12.76% of failures due to overloading in China. The overloading has caused the failure of bridges in the USA as 8.75% (Wardhana & Hadipriono, 2003), 12.71% (Lee et al., 2013), 11.29% (Cook & Barr, 2017) and 13.06% (Taricska, 2014), refer table 1.2. Overloading can be minimised by adopting technologies such as Weigh-In-Motion (WIM) along with structural health monitoring (SHM) systems suitable for a project or network-specific installations (Fiorillo & Ghosn, 2017).

1.1.4.4. Fire

Fires on bridges are commonly caused by the collision of vehicles such as fuel tankers or freight trucks and multiple vehicle collisions or construction accidents ((Bai et al., 2006)(Bai et al., 2006)Garlock et al., 2012). Fire can reach very high temperatures (in the range of 800–

900°C) within the first few minutes of fire initiation and then the temperature can rise to 1000°C or higher in the first 30 min (Garlock et al., 2012)

The rapid rise in temperature can create large thermal gradients in the structural members and consequently cause spalling of the concrete and local buckling of steel members (Peng, 2008). Moreover, fires can lead to a significant decrease in the load-carrying capacity of the structural members due to reduction in the strength and stiffness of materials, which can further lead to partial or full and stiffness of materials, which can further lead to partial or full collapse of bridges (Bai et al., 2006)

Garlock et al. summarize some of the major bridge fire incidents in the past 15 years which are:

- On the Mezcala cable-stayed bridge in Mexico, a traffic incident on March 17th, 2007, involving two school bus and a truck transporting coconut overturned (figure 1.10) and produced a fire at deck level resulting in the failure of one stay cable and limited damage to an adjacent cable. The bridge was immediately closed to traffic and reopened to limited traffic prior to cable replacement.
- Xupu Bridge is a cable-stayed bridge span Huangpu River in Shanghai, China. Since its closing, Xupu Bridge has seen occasional fires in 2008 and 2011. On May 3, 2011, the bridge caught fire due to a chemical tank truck carrying xylene burst into flames (figure 1.11). Similarly, the bridge was immediately closed to traffic (Liu et al., 2012).

Figure 1.10. Truck overturned on Mezcala Bridge (Garlock et al., 2012).

Figure 1.11. Close up of Xupu bridge fire, May 3, 2011 (Liu et al., 2012).

1.1.4.5. Blast

A blast is a process in which energy is dispersed in a very short period of time which is termed an explosion. On a commercial scale and for military purposes, Trinitrotolueme (TNT) is the most commonly used type of explosive. Other types of explosives are the C-4, Triacetone-Triperoxide (TATP), Hexamethlene Triperoxide Diamine (HMTD), (NCTC, 2014).

During an explosion, impact of the explosive and the high velocity impact of exploded fragments cause the primary damage to the structure. Furthermore, the blast waves are released at a very high pressure and in a very short period travelling through the surroundings in a uniform pattern until intercepted by a barrier. This wave propagation will be further explained in Section 1.4.1 (Winget et al., 2005)

- On the 12th of April, 2007 NBC News reported that a suicide truck bomb exploded on the Al-Sarafiya Bridge, a major steel bridge in Baghdad, Iraq (figure 1.12), which led to 26 injuries and 10 deaths (NBC News, 2007).
- Another bridge in Iraq received serious damaged due to a small amount of explosive that was placed at the piers of the bridge, causing the collapse of the pier as shown in figure 1.13.

Figure 1.12. Collapse of the Al-Sarafiya Bridge due to blast (NBC News, 2007).

Figure 1.13. Truck bomb destroys key bridge in western Iraq (NYDN, 2009)

1.1.4.6. Lacks of inspection and maintenance

Usually bridges are designed and constructed to serve for a long time, at least 100 years. However, bridges in service are constantly subject to not only dead and live loads, but also attack by the environment. As a result, bridges experience progressive deterioration, which, when exceeding a certain threshold level, can cause serious problems. The deterioration mechanism is influenced by various factors including material properties, environmental conditions, live load situation (Kim et al., 2013). The risk of bridge deterioration cannot be completely eliminated - however, a good maintenance program including regular inspection and proper rehabilitation will slow down this process (Biezma & Schanack, 2007a). Figure 1.14 shows the collapse of Morandi Bridge Genova.

Figure 1.14. Collapse of Morandi Bridge Genova(De Matteis et al., 2019).

1.2. Collapse mechanisms of bridge due to blast

In this section, the collapse mechanisms due to blast of a two common bridge types, namely, beam bridges and flexible long-span bridges, will be reviewed.

1.2.1. Beam bridges

With the increase in terrorist attacks in recent years, the safety of critical bridges under blast loading has become a public concern and a topic of interest for many researchers. (Yi et al., 2013) conducted a comprehensive series of simulations on the blast effects on three-span simply-supported highway bridges and suggested the following failure mechanisms for the important bridge components:

- Pier: eroding of pier bottom concrete, shearing of a pier from the footing, rebar severance, breakage of pier, spalling of concrete surface, and formation of plastic hinges;
- Bent beam: local failure of concrete under bearings, crushing of concrete, and shear failure;
- Stringer: collapse, and yielding of the steel;
- Deck: crushing under high pressure, dislocation under the effect of the blast wave, and collapse due to loss of support.

They also suggested that not all failure mechanisms may appear during the blast for a particular bridge. The presence of a particular failure mechanism depends on many factors, including the bridge geometry, magnitude of blast loads, standoff distance, the surrounding environment, etc. However, all major mechanisms may be present under high level blast loads,

and the bridge can be damaged completely. It should also be noted that progressive collapse may occur under the effect of a blast, as demonstrated in the failure of a multispan bridge on the Northumberland Strait in Canada due to the loss of a local bridge component during a blast event (Ghali & Tadros, 1997).

For bridges or structural components that need to be designed for intentional or unintentional blast loads, the AASHTO code (AASHTO, 2012) suggests that the following should be considered:

- The size of explosive charge;
- The shape of explosive charge;
- The type of explosive;
- The standoff distance;
- The location of the charge;
- The possible modes of delivery and associated capacities;
- The fragmentation associated with vehicle-delivered explosives.

However, as the size of the explosive charge is unpredictable, the cost of building bridges capable of resisting all possible potential blasts would be very high.

1.2.2. Flexible long-span bridges

The behavior of flexible long-span bridges under blast loading has also been investigated by many researchers. Hao & Tang (2010) performed intensive numerical simulations to investigate the dynamic responses and resulting damages of a cable stayed bridge due to blast loading. They concluded that when the explosion occurs near the towers and piers, the damage to the bridge is mainly induced by the resulting stress wave propagation, and local concrete crushing and spalling are the two main damage modes. By contrast, when the explosion was set away from the bridge, global damage modes (shear and flexural) may result. Therefore more significant damage to the bridge towers and piers may result although the scaled distance is larger. Moreover, catastrophic bridge collapse can be expected if damage to an entire cross section of towers and piers takes place. Son et al. (2005) studied the blast-induced response of the orthotropic steel decks of cable-stayed and suspension bridges and pointed out that the collapse mode of orthotropic steel decks was in the form of buckling in the longitudinal direction due to the P-Δ effect. The axial compressive force P in the deck acting on the downward displacement Δ generated by the blast pressure caused this destabilizing P-Δ effect. Suthar (2007) investigated the effect of the combination of dead, live, and blast loads on a suspension bridge. Based on the bending moments and deformations of the structural members,

the author concluded that although the suspension bridge experienced severe localized damage resulting from the blast load, collapse of the suspension bridge was unlikely for all the blast events considered

1.3. Consequences of bridge failures

The consequences of failure vary significantly from structure to structure, and may depend on a range of factors which are related to the hazard itself, the structure and its utilization, as well as the surrounding environment. First, the source and nature of the hazard leading to the bridge collapse will affect considerably the consequences. It is expected that the greater the magnitude and duration of a hazard, the greater will be the consequences. The bridge type will also influence both its vulnerability and robustness, and, hence, the consequences, which are likely to be sensitive to factors such as the structural form, the material used, age and condition, as well as quality of construction (Garg et al., 2020).

Table 1.3. Categorization of bridge failure consequences (Garg et al., 2020)

Consequence Categories	Examples
Human	Fatalities Injuries Psychological damage
Economic	Replacement / repair costs Loss of functionality / downtime Traffic delay / re-routing costs Traffic management costs Clean up costs Rescue costs Regional economic effects Loss of production / business Investigations / compensations Infrastructure inter-dependency costs
Environmental	CO_2 Emissions Energy use Pollutant releases Environmental clean-up / reversibility
Social	Loss of reputation

	Erosion of public confidence Undue changes in professional practice

1.4. Definition of blast load

An explosion can be defined as a very fast chemical reaction involving a solid, dust or gas, during which a rapid release of hot gases and energy takes place. The phenomenon lasts only some milliseconds and it results in the production of very high temperatures and pressures. Blast wave propagation depends on several parameters such as its impulse, the stand-off distance, weight of explosive. All these parameters will be presented below.

1.4.1. Ideal blast wave characteristics

During detonation the hot gases that are produced expand in order to occupy the available space, leading to wave type propagation through space that is transmitted spherically through an unbounded surrounding medium.

The blast wave contains a large part of the energy that was released during detonation and moves faster than the speed of sound. Figure 1.15 shows the idealised profile of the pressure in relation to time for the case of a free-air blast wave, which reaches a point at a certain distance from the detonation. The pressure surrounding the element is initially equal to the ambient pressure P_o, and it undergoes an instantaneous increase to a peak pressure P_{so} at the arrival time t_A, when the shock front reaches that point. The time needed for the pressure to reach its peak value is very small and for design purposes it is assumed to be equal to zero. The peak pressure P_{so} is also known as side-on overpressure or peak overpressure. The value of the peak overpressure decreases with increasing distance from the detonation centre. After its peak value, the pressure decreases with an exponential rate until it reaches the ambient pressure at t_A+t_o, t_o being called the positive phase duration. After the positive phase of the pressure-time diagram, the pressure becomes smaller (referred to as negative) than the ambient value, and finally returns to it. The negative phase is longer than the positive one, its minimum pressure value is denoted as P_{so}^- and its duration as t_o^-. During this phase the structures are subjected to suction forces, which is the reason why sometimes during blast loading glass fragments from failures of facades are found outside a building instead in its interior.

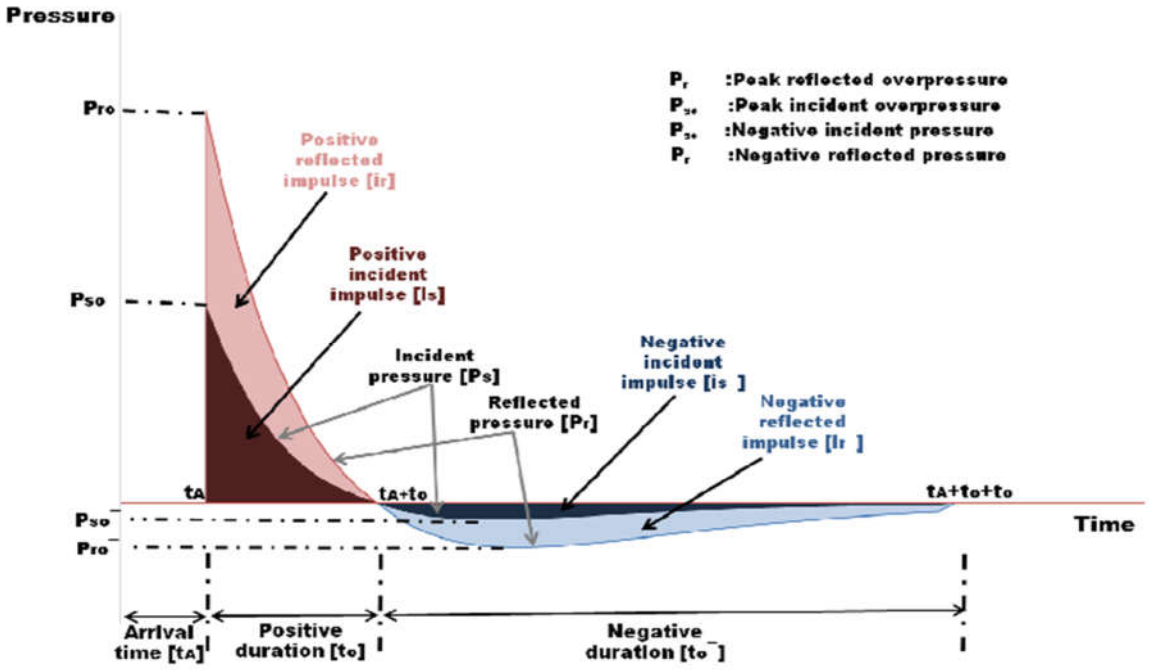

Figure 1.15. Incident and reflected pressure time histories (Karlos et al., 2016)**.**

The negative phase of the explosive wave is usually not taken into account for design purposes as it has been verified that the main structural damage is connected to the positive phase. As can be seen from figure 1.15, the positive incident pressure decreases exponentially. The following form of Friedlander's equation 1.1 has been proposed and is widely used to describe this rate of decrease in pressure values:

$$P_s(t) = P_{s0}\left(1 - \frac{t}{t_0}\right)e^{-b\frac{t}{t_0}} \qquad \textbf{(1.1)}$$

Where :

P_{so}	is the peak overpressure
t_o	is the positive phase duration
b	is a decay coefficient of the waveform
t	is the time elapsed, measured from the instant of blast arrival

The decay coefficient b can be calculated through a non-linear fitting of an experimental pressure time curve over its positive phase. Besides the peak pressure, for design purposes an even more important parameter of the blast wave pulse is its impulse because it relates to the total force (per unit area) that is applied on a structure due to the blast. It is defined as the shaded area under the overpressure-time curve of figure 1.15. The impulse is distinguished into positive i_s and negative i_s^-, according to the relevant phase of the blast wave time history. Equation 1.2 gives the expression in the case of the positive impulse, which is more significant than its negative counterpart in terms of building collapse prevention.

$$i_s = \int_{t_A}^{t_A+t_o} P_s(t)dt \tag{1.2}$$

For equation (1.1), the positive impulse can be analytically calculated as:

$$i_s = \frac{P_{so}t_o}{b^2}[b - 1 + e^{-b}] \tag{1.3}$$

This equation constitutes an alternative way for solving iteratively for the decay parameter b when the values of i_s, P_{so} and t_o are known from experimental data.

1.4.2. Blast parameters

The principal blast loads parameters are stand-off distance and explosive type and weight.

1.4.2.1. Stand-off distance

One of the most critical parameters for blast loading computations is the distance of the detonation point from the structure of interest. The peak pressure value and velocity of the blast wave, which were described earlier, decrease rapidly by increasing the distance between the blast source and the target surface (figure 1.16). In the figure, only the positive phases of the blast waves are depicted, whose durations are longer whenever the distance from the detonation point increases.

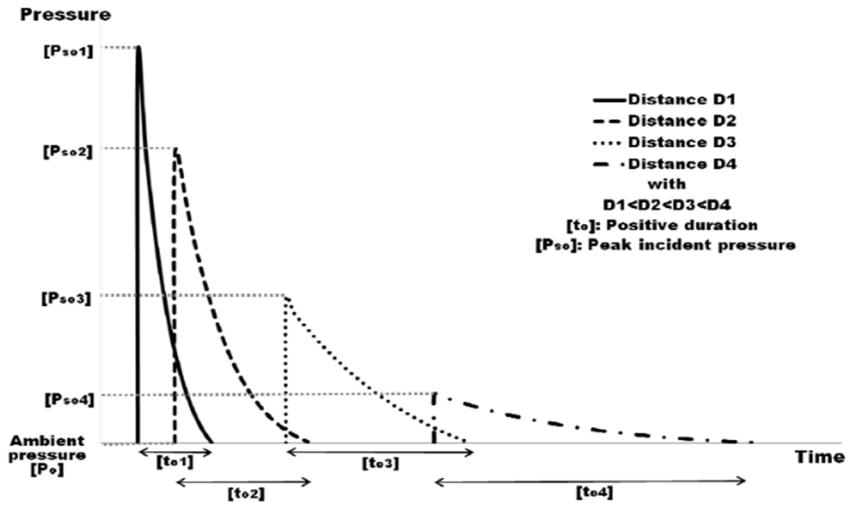

Figure 1.16. Influence of distance on the blast positive pressure phase (Karlos et al., 2016)**.**

The effect of distance on the blast characteristics can be taken into account by the introduction of scaling laws. According to Hopkinson-Cranz law, a dimensional scaled distance is introduced as described by equation 1.4.

$$Z = \frac{R}{\sqrt[3]{W}} \tag{1.4}$$

Where:

R the distance from the detonation source to the point of interest.

W the weight of the explosive.

1.4.2.2. Explosive type and weight

The wide variety of explosives has led to the adoption of a universal quantity, which is used for all necessary computations of blast parameters. TNT (Trinitrotoluene) was chosen as its blast characteristics resemble those of most solid type explosives. An equivalent TNT weight is computed according to 1.5 that links the weight of the chosen design explosive to the equivalent weight of TNT by utilizing the ratio of the heat produced during detonation:

$$W_e = W_{exp} \frac{H^d_{exp}}{H^d_{TNT}} \tag{1.5}$$

Where:

W_e is the TNT equivalent weight

W_{exp} is the weight of the actual explosive

H^d_{exp} is the heat of detonation of the actual explosive

H^d_{TNT} is the heat of detonation of the TNT

1.4.3. Blast pressure determination

There are various relationships and approaches for determining the incident pressure value at a specific distance from an explosion. All the proposed relationships entail computation of the scaled distance, which depends on the explosive mass and the actual distance from the centre of the spherical explosion.

Kinney and Graham (1985) present a formulation that is based on chemical type explosions. It is described by equation 1.6 and has been used extensively for computer calculation purposes.

$$P_{so} = P_0 \frac{808\left[1 + \left(\frac{Z}{4.5}\right)^2\right]}{\left\{\left[1 + \left(\frac{Z}{0.048}\right)^2\right]\left[1 + \left(\frac{Z}{0.32}\right)^2\right]\left[1 + \left(\frac{Z}{1.35}\right)^2\right]\right\}^{0.5}} \tag{1.6}$$

Where:

Z is the scaled distance

P_o is the ambient pressure

Other relationships for the peak overpressure for spherical blast include those of (Brode, 1955) shown in Equations 1.7.a and 1.7.b. The pressure P_{so} in bars:

$$P_{so} = \begin{cases} \frac{6.7}{Z^3} + 1 & , for \quad P_{so} > 10\ bar \\ \frac{0.975}{Z} + \frac{1.455}{Z^2} + \frac{5.85}{Z^3} - 0.019 & , for \quad 0.1 < P_{so} < 10 bar \end{cases} \quad \textbf{(1.7.a)} \quad \textbf{(1.7.b)}$$

Another formulation, that is widely used for computing peak overpressure values for ground surface blast has been proposed by Newmark and does not contain categorization according to severity of the detonation:

$$P_{so} = 6784\frac{W}{R^3} + 93\sqrt{\frac{W}{R^3}} \quad \textbf{(1.8)}$$

where, P_{so} is in bars,

W is the charge mass in metric tons (=1000kg) of TNT and

R is the distance of the surface from the center of a spherical explosion in m.

Mills (1987) has also introduced an expression of the peak overpressure in kPa, in which W is expressed in kg of TNT and the scaled distance Z is in $m/kg^{1/3}$, which reads:

$$P_{so} = \frac{1772}{Z^3} - \frac{114}{Z^2} + \frac{108}{Z} \quad \textbf{(1.9)}$$

Figure 1.17 shows a set of analytical relationships providing the above blast parameters in terms of polynomial functions of the logarithm of the scaled distance. Hence, the time of arrival can be determined.

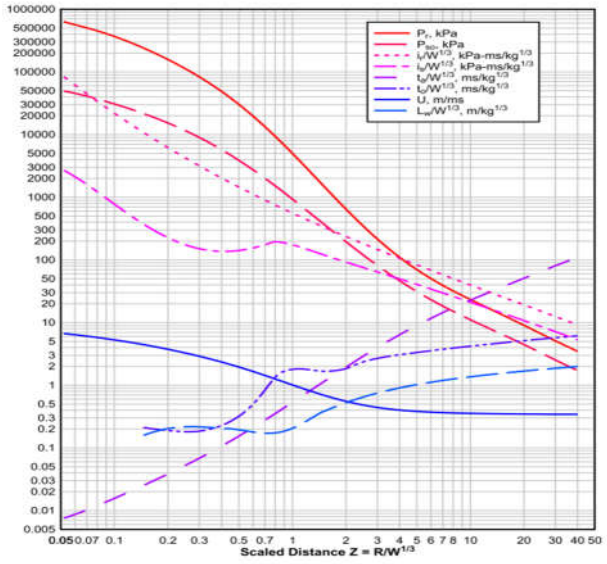

Figure 1.17. Parameters of positive phase of shock spherical wave of TNT charges from free-air bursts (Karlos et al., 2016)**.**

1.4.4. Explosion and blast-loading types

As shown in figure 1.18, they can be distinguished in three basic types, which depend on the relative position of the explosive source and the structure to be protected i.e., on the height H* above ground, where the detonation of a charge W occurs, and on the horizontal distance RG between the projection of the explosive to the ground and the structure. These three explosion types are:

(a) **Free-air bursts:** The explosive charge is detonated in the air; the blast waves propagate spherically outwards and impinge directly onto the structure without prior interaction with other obstacles or the ground.

(b) **Air bursts:** The explosive charge is detonated in the air, the blast waves propagate spherically outwards and impinge onto the structure after having interacted first with the ground: a Mach wave front is created.

(c) **Surface bursts:** The explosive charge is detonated almost at ground surface; the blast waves immediately interact locally with the ground and they next propagate hemi-spherically outwards and impinge onto the structure.

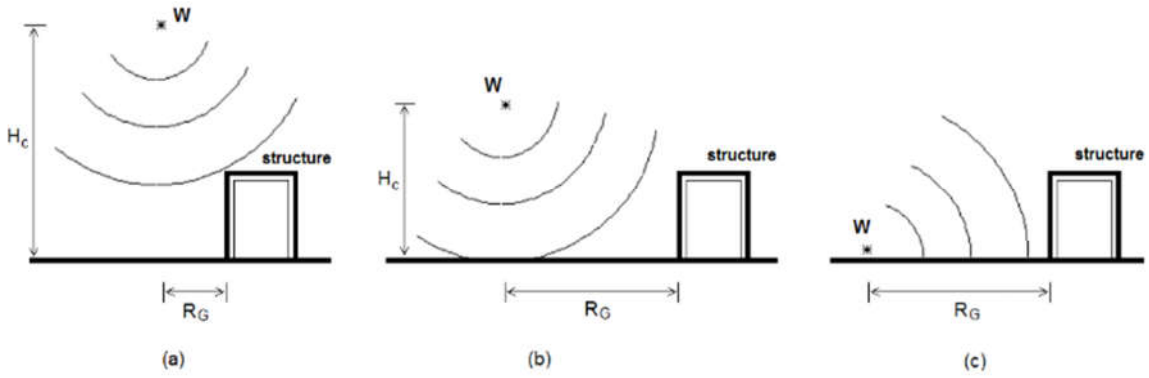

Figure 1.18. Types of external explosions and blast loadings (Karlos et al., 2016)**.**

Conclusion

In this chapter, the causes of bridge collapse, particularly blast, were the main focus. To achieve this objective, the causes of bridge collapse, the mechanisms of bridge collapse due to blast, the consequences of bridge collapse as well as the definition of blast load have been reviewed.

CHAPTER 2: METHODOLOGY

Introduction

The literature review presented in the first chapters gives us more knowledge about the causes of bridge collapse, the mechanism of collapse due to blast loading, the consequences of bridge failures and the definition of blast loading. The methodology is the part of the study that establishes the research procedure after the definition of the problem, in order to achieve the set objectives. The content of this chapter is divided into four main parts. Firstly, a general recognition of the site through a literature search. Secondly, the collection of data that will help us to model and analyse the bridge. Then, this chapter will focus on a detailed presentation of the analytical and numerical methods for the static analysis based on the Eurocodes and the dynamic analysis procedure. Finally, with the analysis done, an overview of the software used in this thesis and the modelling will be done.

2.1. Site recognition

The general recognition of site of the building will be done from literature search whose essential goal is to know physical parameters specially the geographic location and climate, relief and ground in one side, and socio-economic parameters in the other side.

2.2. Data collection

The main type of data required for the purpose of this research is the geometrical and statistical data of the bridge.

2.2.1. Geometrical data

Geometrical data will be taken from plans in order to outcome different views of bridge. They show geometry of structural elements and surface area. Necessary steel reinforcement in slab will be presented after.

2.2.2. Statistical data

The collection of statistical data will present mainly the characteristics of materials. It concerns concrete and reinforcement.

2.3. Methodology

A common situation in structural mechanics is that a structure is only affected by static forces. If the structure is affected by a dynamic force (a force that varies with time), it may have a different response compared with the response of a static force. This section is dedicated to procedures used to outcome bridge reactions under static and dynamic loads.

2.3.1. Preliminary design

In order to have sections of structural elements, a preliminary design has been done according to some principles mentioned in section. Final sections of each element in this part will be presented.

2.3.2. Static and dynamic loading

Different types of actions act on the bridge. In the study, only permanent, variable and blast loads will be considered on the bridge. Regarding the study, the permanent, variable and blast loads will be considered. Permanent loads are represented by $G_{k,j}$; $Q_{k,i}$ express variable loads and A_d the accidental load.

2.3.2.1. Load combinations

A load combination defines a set of designed values used for the verification of the structural reliability for a limit state under the simultaneous influence of different actions. The designed value is the value obtained by multiplying the representative value by a partial factor.

a) Eurocodes

The main codes applied in this thesis are:

- EN 1990 Eurocode: Basis of structural design ;
- EN 1991 Eurocode 1: Actions on structures ;
- EN 1992 Eurocode 2: Design of concrete structures ;
- EN 1997 Eurocode 7: Geotechnical design.

b) Static load cases

As recommended in EN 1990, the following rules have been considered for the combination of loads with respect to static loads applied in a structure. In the case of a bridge, the following sections show.

i. Partial Factors for Load Combinations

Table 2.1 gives the values of the partial safety factors with respect to each load type.

Table 2.1. Partial factors for load combinations.

Partial factors	G_1	G_2	P	ε_2	T_K	TS	UDL	F_w
γ	1.35	1.5	1	1.2	1.5	1.35	1.35	1.5
ψ_o	/	/	/	/	0.6	0.75	0.4	0.6
ψ_1	/	/	/	/	0.6	0.75	0.4	0.2
ψ_2	/	/	/	/	0.5	0	0	0

ii. Fundamental combination

This combination is used for Ultimate Limit State (ULS) in transient design situation associated to determining of structure resistance and is given by equation 2.1:

$$\sum_j \gamma_{G,j} \times G_{k,j} + \gamma_{Q,1} \times Q_{k,1} + \sum_{i>1} \gamma_{Q,i} \times \psi_{0,i} \times Q_{k,i} \quad \textbf{(2.1)}$$

a) When the traffic load is considered as the leading variable action;

$$Q_{k,1} = 1.35 \times G_1 + 1.5 \times G_2 + 1.2 \times S + 1.35 \times (TS + UDL) + 1{,}5 \times 0{,}6 \times T_k + 1{,}5 \times 0{,}6 \times F_w \quad \textbf{(2.2)}$$

b) When the wind load is considered as the leading variable action and the traffic load is considered as the accompanying variable action

$$Q_{k,1} = 1.35 \times G_1 + 1.5 \times G_2 + 1.2 \times S + 1.35 \times (0.75 \times TS + 0.4 \times UDL) + 1{,}5 \times 0{,}6 \times T_k + 1{,}5 \times F_w \quad \textbf{(2.3)}$$

iii. Characteristic combination (rare)

Usually used for non-reversible Serviceability Limit States (SLS), this combination (2.4) has to be used in the verifications with the allowable stress method:

$$\sum_j G_{k,j} + P + Q_{k,1} + \sum_{i>1} \psi_{0,i} \times Q_{k,i} \quad \textbf{(2.4)}$$

$$Q_{k,1} = G_1 + G_2 + (TS + UDL) + 0{,}6 \times (T_k + F_w) \quad \textbf{(2.5)}$$

iv. Frequent combination

Frequent combination 2.6 is recommended for reversible SLS:

$$\sum_j G_{k,j} + P + \psi_{1,1} \times Q_{k,1} + \sum_{i>1} \psi_{2,i} \times Q_{k,i} \quad \textbf{(2.6)}$$

$$Q_{k,1} = G_1 + G_2 + S + (0.75 \times TS + 0.4 \times UDL) + 0{,}5 \times T_k \quad \textbf{(2.7)}$$

$$Q_{k,1} = G_1 + G_2 + S + 0.2 \times F_w + 0{,}5 \times T_k \quad \textbf{(2.8)}$$

v. Quasi-permanent combination

Generally used for long-term effects, it is given by equation 2.9:

$$\sum_j G_{k,j} + P + \sum_{i \geq 1} \psi_{2,i} \times Q_{k,i} \quad \textbf{(2.9)}$$

$$Q_{k,1} = G_1 + G_2 + S + (0.75 \times TS + 0.4 \times UDL) + 0{,}5 \times T_k \quad \textbf{(2.10)}$$

c) Dynamic load cases

This combination is used for Ultimate Limit State (ULS) in accidental design situation associated to determining of structure resistance and is given by equation 2.10:

$$\sum_j G_{k,j} + A_d + (\psi_{1,1} \text{ or } \psi_{2,1})Q_{k,1} + \sum_{i>1} \psi_{2,i} \times Q_{k,i} \quad \textbf{(2.11)}$$

When the traffic load is considered as the leading variable action;

$$Q_{k,1} = G_1 + G_2 + (0.75 \times TS + 0.4 \times UDL) + 0{,}6 \times (T_k + 0.6 \times F_w) \quad \textbf{(2.12)}$$

Where:

G: is the self-weight of the structure;

A_d: is the design value of the accidental load (in this case the blast load);

$Q_{k,1}$: is the characteristic value of the leading variable load;

$Q_{k,i}$: are the characteristic values of the accompanying variable loads.

The values of ψ_1 and ψ_2 depend on the relevant accidental design situation.

2.3.2.2. Load actions

This section focuses on the calculation of loads acting on the bridge. These loads include: permanent and variable loads. Blast load and its parameters will also be presented.

a. Permanent loads

Dead loads represent actions which remain relatively constant over the structure life cycle. They comprise the weight of bridge's structural elements (g_1) such as girders, slab, and the others. Weight of non-structural elements (g_2), (barriers, road pavement …) are also included in dead loads.

b. Live loads

The live load on the bridge is moving load throughout bridge length. The moving loads are vehicles, pedestrians, etc.

i. Number of lanes

The number and the width of notional lanes result from table. 2.3 (*EN 1991-2*, 2003).

Tableau 2.1. Multipliers for the characteristic values of variable loads (*EN* 1991-*2*, 2003).

Carriageway width w	Number of notional lanes	Width of a notional lane w_l	Width of the remaining area
$w < 5{,}4$ m	$n_l = 1$	3 m	$w - 3$ m
$5{,}4$ m $\leq w < 6$ m	$n_l = 2$	$\frac{w}{2}$	0
6 m $\leq w$	$n_l = Int\left(\frac{w}{3}\right)$	3 m	$w - 3 \times n_l$
NOTE For example, for a carriageway width equal to 11m, $n_l = Int\left(\frac{w}{3}\right) = 3$, and the width of the remaining area is 11 - 3×3 = 2m.			

ii. Traffic loads

For the complete analysis of the vertical forces, the traffic Load Model 1 (LM1) has been considered. This Load Model is constituted of a tandem load (TS) and a uniformly distributed load (UDL), (see *EN 1991-2*, 2003). The class of the bridge is class 3. Table. 2.4 recaps the values to consider for loads due to traffic.

Tableau 2.2. Characteristic values of load model 1 (EN 1991-2, 2003).

Location	Tandem system *TS*	*UDL* system
	Axle loads Q_{ik} (kN)	AC1 q_{ik} (or q_{rk}) (kN/m^2) AC1
Lane Number 1	300	9
Lane Number 2	200	2,5
Lane Number 3	100	2,5
Other lanes	0	2,5
Remaining area (q_{rk})	0	2,5

Correction factors α_{Qik}, α_{qik}, α_{qr}, to be considered are shown in table 2.5:

Tableau 2.3. Values of adjustment factors (*EN 1991-2*, 2003).

	α_{Q1}	$\alpha_{Qi}\ i \geq 2$	α_{q1}	$\alpha_{qi}\ i \geq 2$	α_{qr}
1st class	1	1	1	1	1
2nd class	0,9	0,8	0,7	1	1
3rd class	0,8	0,5	0,5	1	1

In what follows, the load group gr1a in table. 3.6 will be adapted. It is represented by equation (2.13).

$$gr1a = TS_k + UDL_k + q*_{fk} \tag{2.13}$$

Where $q*_{fk}$ represents the uniformly distributed load on footways and cycle tracks.

Tableau 2.4. Assessment of groups of traffic loads (EN 1991-2, 2003).

		CARRIAGEWAY						FOOTWAYS AND CYCLE TRACKS
Load type		Vertical forces				Horizontal forces		Vertical forces only
Reference		4.3.2	4.3.3	4.3.4	4.3.5	4.4.1	4.4.2	5.3.2-(1)
Load system		LM1 (TS and UDL systems)	LM2 (Single axle)	LM3 (Special vehicles)	LM4 (Crowd loading)	Braking and acceleration forces [a]	Centrifugal and transverse forces [a]	Uniformly Distributed load
Groups of Loads	gr1a	Characteristic values						Combination value [b]
	gr1b		Characteristic value					
	gr2	Frequent values				Characteristic value	Characteristic value	
	gr3 [d]							Characteristic value [c]
	gr4				Characteristic value			Characteristic value
	gr5	See annex A		Characteristic value				
	Dominant component action (designated as component associated with the group)							

[a] May be defined in the National Annex (for the cases mentioned).
[b] May be defined in the National Annex. The recommended value is 3 kN/m².
[c] See 5.3.2.1-(2). One footway only should be considered to be loaded if the effect is more unfavourable than the effect of two loaded footways.
[d] This group is irrelevant if gr4 is considered.

c. Wind load

The general expression of wind force F_w acting on a structure or a structural component can be determined directly by using equation 2.14.

$$F_w = c_s.c_d.c_f.q_p(z_e).d_{tot} \tag{2.14}$$

Where:

$q_p(z_e)$ is the peak velocity pressure at reference height Ze

d_{tot} is the total depth of the structural element z_e

$c_s.c_d$ is the structural factor

c_f is the force coefficient

The peak velocity pressure at height z is expressed by equation 2.15:

$$q_p(z) = \frac{1}{2}.\left(1 + 7.I_v(z)\right).\rho.v_m^2(z) = c_e(z).q_b \quad \textbf{(2.15)}$$

Where:

ρ is the air density

$v_m(z)$ is the mean wind velocity at height z and is given by equation 2.17

$$v_m(z) = c_r(z).c_o(z).v_b \quad \textbf{(2.16)}$$

$c_r(z)$ is the roughness coefficient

$c_o(z)$ is the orography coefficient

v_b is the basic wind velocity given by equation (2.18)

$I_v(z)$ is the turbulence intensity and can be obtained from equation (2.17)

$$(I_v(z) = \frac{k_l}{c_o(z).ln(z/z_o)} \quad \textbf{(2.17)}$$

k_l is the turbulence factor

z_0 is the roughness length

$$v_b = c_{dir}.c_{season}.v_{b,0} \quad \textbf{(2.18)}$$

c_{dir} is the direction factor

c_{season} is the season factor

Roughness length and coefficients depends on terrain category and parameters. The procedure to find values of different coefficients is detailed in (*EN 1991-1-4*).

The wind used for design will be wind acting on a loaded bridge.

d. Thermal action

According to the vertical linear component approach, a temperature variation of ΔT between the top and bottom of the slab, the effect of this temperature variation results in stresses at the top and bottom of the beam.

Table 2.2. Values of K_h depending on h_o(EN-1992-1-1_2, 2009).

h_0	k_h
100	1.0
200	0.85
300	0.75
≥ 500	0.70

To calculate these stresses, the resulting force and moment due to temperature change have to be evaluated and calculate these stresses, the resulting force and moment due to temperature change have to be evaluated.

$$N = A_c \varepsilon E_{cm} \quad \textbf{(2.19)}$$

$$\varepsilon = \alpha \Delta T \quad \textbf{(2.20)}$$

Where:

α is the coefficient of thermal expansion for concrete;

A_c is the area of slab section;

ΔT is the temperature variation;

ε is the strain due to temperature difference.

Table 2.3. Recommended values of linear temperature difference component for different types of bridge decks for road, foot and railway bridges (EN-1992-1-1_2, 2009).

Type of Deck	Top warmer than bottom	Bottom warmer than top
	$\Delta T_{M,heat}$ (°C)	$\Delta T_{M,cool}$ (°C)
Type 1: Steel deck	18	13
Type 2: Composite deck	15	18
Type 3: Concrete deck:		
- concrete box girder	10	5
- concrete beam	15	8
- concrete slab	15	8

The values given in the table are based on a depth of surfacing of 50 mm for road and railway bridges.

e. Creep and shrinkage

i. Creep

The effects of creep are taken into account by reducing concrete elastic modulus E_{cm} thus increasing the modular ratio.

Modular ratio at infinite time n_L is given by equation 2.21

$$n_L = n_0(1 + \psi_L \rho_t) \quad \textbf{(2.21)}$$

Where:

n_0 is the modular ratio E_s/E_{cm} for the short-term loading

ρ_t is the creep coefficient depending on the age t of concrete and the age t_0 at loading

ψ_L is the creep multiplier depending on the type of loading ; to be taken as 1,1 for permanent loads ; 0,55 for primary and secondary effects of shrinkage ; 1,5 for pre-stressing by imposed deformations.

In order to determine the creep coefficient $\rho(t, t_0)$, the following data will be assumed or calculated:

Relative humidity	RH=70%
Reference zero time	t_0= 3 days
Fictitious dimension	h=2Ac/u

The value of $\rho(t, t_0)$ total shrinkage at $t=\infty$ will be found with software MIDAS/civil 2022.

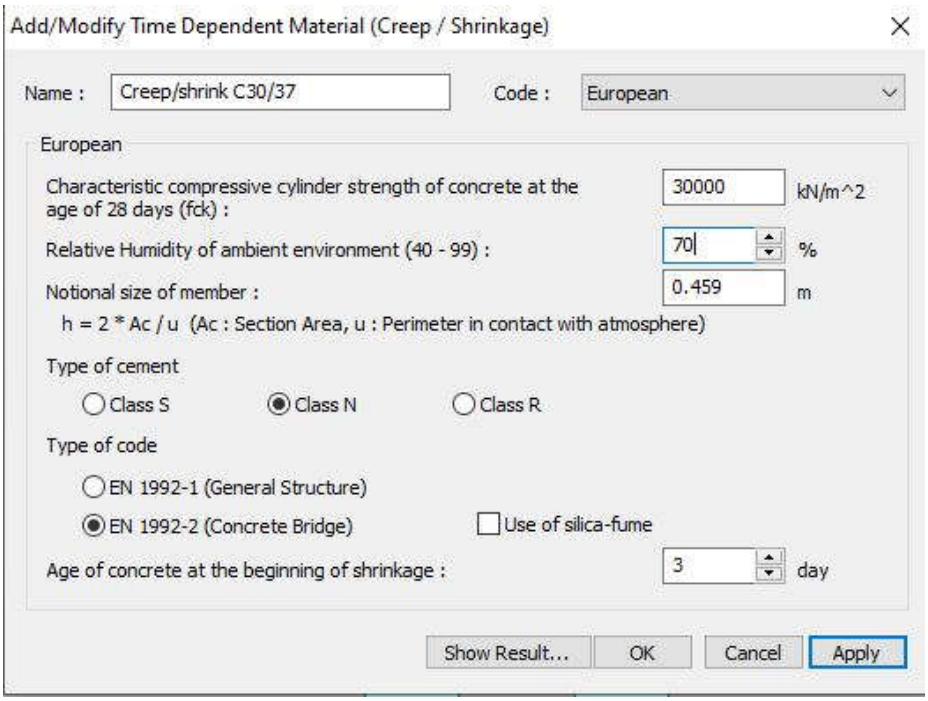

Figure 2.1. Time dependent concrete (MIDAS/civil 2022 software).

ii. Shrinkage

Total shrinkage at infinite is calculated through equation 2.22

$$\varepsilon_{cs}(\infty) = \varepsilon_{ca}(\infty) + \varepsilon_{cd}(\infty) \quad \textbf{(2.22)}$$

$$\varepsilon_{ca} = 2.5.(f_{ck} - 10).10^{-6} \quad \textbf{(2.23)}$$

$$\varepsilon_{cd}(\infty) = k_h.\varepsilon_{c0} \quad \textbf{(2.24)}$$

$$\varepsilon_{c0} = 0.85.((220 + 110.\alpha_{ds1}).e^{(-\alpha ds2.f_{cm}/f_{cm0})}).10^{-6}.\beta_{RH} \quad \textbf{(2.25)}$$

$$\beta_{RH} = 1.55.\left(1 - \left(\frac{RH}{RH_0}\right)^3\right) \quad \textbf{(2.26)}$$

Where:

$\varepsilon_{cd}(\infty)$ is the dry shrinkage strain at infinite

$\varepsilon_{ca}(\infty)$ is the autogeneous shrinkage

Shrinkage of concrete is taken into account by applying an axial force at slab ends. It is given by equation 2.27

$$N_{c,r\infty} = \varepsilon_{cs}(\infty).E_{c,eff}.A_c \quad \textbf{(2.27)}$$

Where $E_{c,eff}$ is the reduced modulus of elasticity for concrete and obtained from equation 2.28

$$E_{c,eff} = \frac{E_{cm}}{1 + \rho(\infty, t_0)} \quad \textbf{(2.28)}$$

The temperature load has to apply the force N_{beam} that will be considered is taken from equation 2.29

$$N_{beam} = N_{c,r\infty}/n \quad \textbf{(2.29)}$$

Where n is the number of beams

f. Blast load

Blast loads are complex in nature. With the help of experimental results and scaling laws, charts are provided in the manual to calculate the blast load parameters for a given charge weight and standoff distance. The empirical formula to find the scaled distance, Z (m), is mentioned in the equation 2.30.

$$Z = \frac{R}{\sqrt[3]{W}} \quad \textbf{(2.29)}$$

Here, R = Standoff distance (m), W = Equivalent TNT weight of explosion (kg).

i. Stand-off distance

Considering figure 2.3 below, the method used to determine the blast load parameters at point A is explained below.

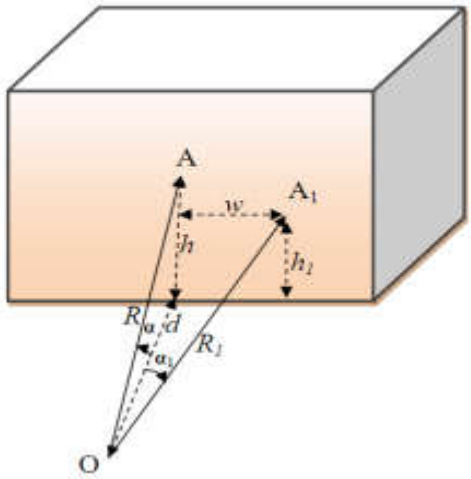

Figure 2.2. Scheme for blast parameters determination (Mbakop, 2020).

The blast origin is point O in figure 2.3, point A is the point where the blast parameters need to be calculated. It is located relative to point O at a horizontal distance d and at a height h. The angle of incidence is α which is the angle made between the shock wave and the line perpendicular to the target surface. The expressions of R and α are given by equations 2.30 and 2.31 respectively.

$$R = \sqrt{(d^2 + h^2)} \tag{2.30}$$

$$\alpha = \cos^{-1}\left(\frac{d}{R}\right) = \tan^{-1}\left(\frac{h}{d}\right) \tag{2.31}$$

ii. Arrival time

Figure 2.4 describes all the required positive phase parameters in metric units with respect to the scaled distance Z. Hence, arrival time can be deduced.

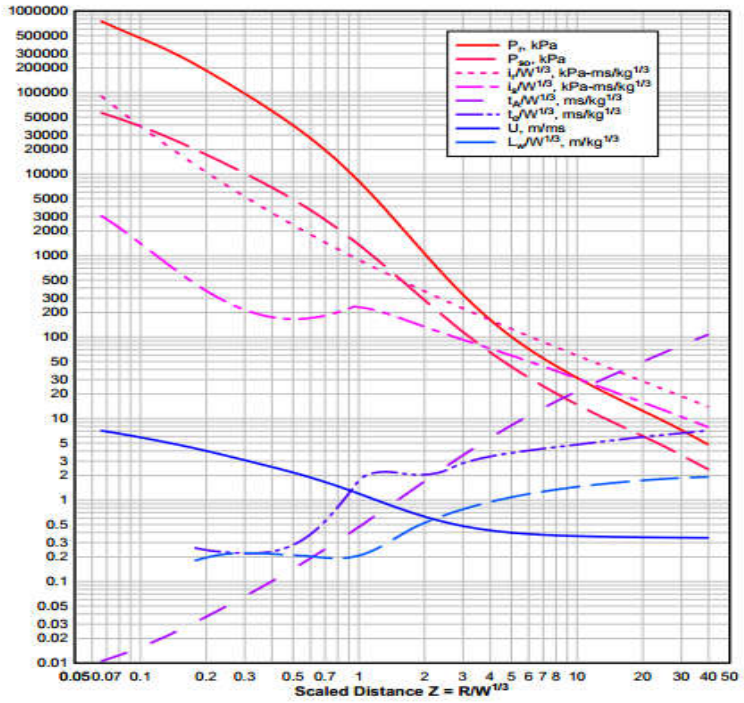

Figure 2.3. Positive phase parameters of shock hemispherical wave of TNT charges from surface bursts (TM5-1300 1990).

iii. Pressure distribution

Using the scaled distance Z and the charts in TM 5-1300, Eric Jacques, an assistant professor at Virginia Tech developed a computer program names RCBlast to calculate the blast loads for known values of charge weight and stand-off distance but it is for W>0.3kg. Excel sheet is used to determine the equivalent blast pressure distribution due to an explosion. The peak pressure is determined with Mills expression 2.32.

$$P_{s0} = \frac{1}{Z}(108 + \frac{1772}{Z^2} - \frac{114}{Z^2}) \qquad (2.32)$$

2.3.3. Static analysis

2.3.3.1. Ultimate limit state

Ultimate limit states are those that relate to the failure of a structural member or a whole structure.

a. Girder design

i. Bending moment design

Steel reinforcement is computed for the section of T beam as display in figure 2.5.

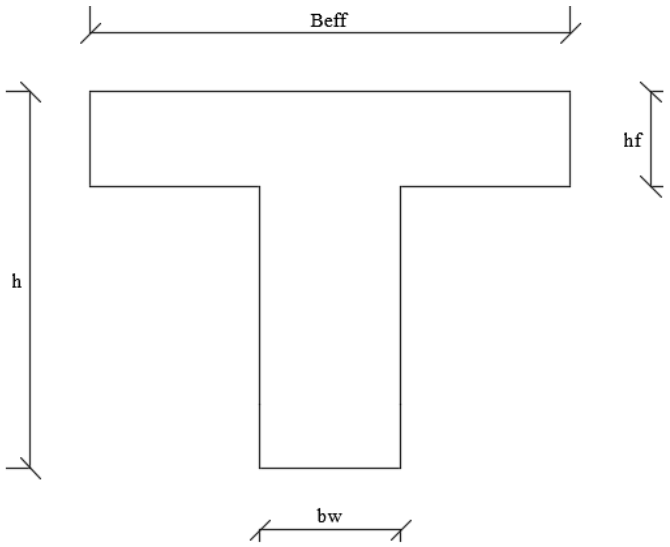

Figure 2.4. The section of T beam.

The longitudinal reinforcement at each point is computed using equation 2.33.

$$A_s = \frac{M_{ed}}{0.9 \times d \times f_{yd}} \tag{2.33}$$

The section of steel obtained has to verify the provision in Eurocode 2 on the maximum and minimum longitudinal reinforcement described by equation 2.34 and 2.35 respectively.

$$A_{s,min} = max\left(0.26\frac{f_{ctm}}{f_{yk}}b_t d; 0.0013 b_t d\right) \tag{2.34}$$

$$A_{s,max} = 0.04 A_c \tag{2.35}$$

Where

b_t: is the mean width of the tension zone;

d: is the effective depth of the section;

f_{ctm}: is the tensile strength of the concrete;

f_{yk}: is the characteristic strength of steel;

f_{yd}: is the design yielding strength of steel.

The verification of the section is done by calculating the resisting bending moment of the section using the position of the neutral axis inside the section. The position of the neutral axis is computed using the equation 2.36.

$$x = \frac{d}{2\beta_2} - \sqrt{\left(\frac{d}{2\beta_2}\right)^2 - \frac{M_{ED}}{\beta_1 \beta_2 b f_{cd}}} \tag{2.36}$$

d: is the effective depth of the section;

b: is the width of the section;

f_{cd}: is the design compressive strength of the concrete;

β_1: is a correction factor equal to 0.81;

β_2: is a correction factor equal to 0.41.

The resisting moment is computed using the equation 2.37:

$$M_{RD} = A_{s,provided} f_{yd}(d - \beta_2 x) \quad \textbf{(2.37)}$$

Where

$A_{s,provided}$: is the effective area of steel reinforcement;

f_{yd}: is the design yielding strength of steel.

ii. Shear design

Transversal reinforcement needs to be inserted in the section to overtake shear forces. From the envelope curve of shear solicitations, the design shear value V_{ED} is obtained and used for different calculations. The necessity of shear reinforcement is computed by comparing the design shear value V_{ED} with the normalised shear capacity of concrete V_{Rdc}. If no shear reinforcement is necessary, the conditions described in equation 2.36 should be satisfied.

$$V_{ed} < V_{Rdc} \quad \textbf{(2.38)}$$

With

$$V_{Rdc} = max \begin{cases} \left[C_{Rdc} k (100 \rho_1 f_{ck})^{1/3} + k_1 \sigma_{cp}\right] b_w d \\ \left[0.035 k^{3/2} {f_{ck}}^{1/2} + k_1 \sigma_{cp}\right] b_w d \end{cases} \quad \textbf{(2.39)}$$

Where:

$k = 1 + \sqrt{\frac{200}{d}} \leq 2.0$: d in mm;

$k_1 = 0.15$;

$\sigma_{cp} = \frac{N_{ED}}{A_c} < 0.2 f_{cd}$ which represent the stress due to axial force;

d: is the effective depth of the section;

b_w: is the smallest width of the section;

$\sigma_{cp} = \frac{A_{s,provided}}{b_w d} \leq 0.02$: reinforcement ration;

$\sigma_{cp} = \frac{0.18}{\gamma_c}$.

When equation 2.38 is satisfied, the minimum reinforcement is used. Otherwise, the resisting strength is computed using equation 2.40.

$$\theta = \frac{1}{2} arcsin\left(\frac{2V_{ED}}{0.9\alpha_{cw} f_{cd} v_1 d b_w}\right) \quad \textbf{(2.40)}$$

$$\frac{A_{sw}}{s} = \frac{V_{ED}}{0.9 d f_{ywd} ctg\theta^2} \quad \textbf{(2.41)}$$

$$V_{Rd} = \min(0.9 d b_w \alpha_{cw} f_{cd} v_1 \frac{(ctg\alpha + ctg\theta)}{1 + ctg^2\theta}; \frac{A_{sw}}{s} z f_{ywd} cot\theta) \quad \textbf{(2.42)}$$

Where

V_{Rd}: resisting shear

A_{sw}: area of the web reinforcement

f_{ywd}: design yield stress of the shear reinforcement

θ: inclination of the cracks or the concrete struts

α: angle between the shear reinforcement and the axis of the design element (α = 90° for stirrups)

f_{cd}: design value concrete compressive strength

s: stirrup spacing

a_{cw}: coefficient of interaction between compressive stresses which can be assumed = 1 for non pre stressed structures

v_1: reduction coefficient for shear cracked concrete (v_1 = 0.6 for $f_{ck} \leq 60\ N/mm2$).

b. Pier design

Column design is done at ULS for the axial force, the bending and the shear force and the verification is done for the slenderness. The solicitations required for the design are obtained from the 3D model. In this work, the bridge will be modelled using the software Midas/civil 2022.

i. Bending moment-axial force verification

The envelope of the bending moment and the axial force solicitations is obtained, the design is done through the M-N interaction diagram. The column's pier strength interaction diagram is a curve of plot points in which each point has two ordinates. The first ordinate is bending moment Slenderness verification strength and the second is the corresponding axial force. For each level, the maximum M-N stresses must belong to the M-N interaction diagram of the section considered. The section used to compute the M-N interaction diagram at different point are as follows.

- **First point**

The section is completely subjected to tension; hence, the concrete is not reacting. $\varepsilon_s = \varepsilon_{su}$, $\varepsilon_{s'} = \varepsilon_{syd}$ then $\sigma_s = \sigma_{s'} = f_{yd}$ are imposed. The limit axial force and bending moment are obtained from the equations 2.43 and 2.44 respectively.

$$N_{Rd} = f_{yd}A_s + f_{yd}A'_s \quad \textbf{(2.43)}$$

$$M_{Rd} = f_{yd}A_s\left(\frac{h}{2} - d'\right) + f_{yd}A'_s\left(\frac{h}{2} - d'\right) \quad \textbf{(2.44)}$$

- **Second point**

The section is completely subjected to tension; hence, the concrete is not reacting. $\varepsilon_s = \varepsilon_{su}$, $\varepsilon_c = 0$ are imposed. The upper steel has to be verified if yielded or not. The value of the limit axial force and bending moment at this point are computed using equation 2.43 and 2.44.

- **Third point**

N is imposed failure due to concrete and the lower reinforcement is yielded. $\varepsilon_s \geq \varepsilon_{syd}$, $\varepsilon_c = \varepsilon_{cu}$ Then, computing the neutral axis, N_{Rd} and M_{Rd} can be computed using respectively equations 2.45 and 2.46.

$$N_{Rd} = -\beta_1 b x f_{cd} + f_{yd}A_s - f_{yd}A'_s \quad \textbf{(2.45)}$$

$$M_{Rd} = f_{yd}A_s\left(\frac{h}{2} - d'\right) + f_{yd}A'_s\left(\frac{h}{2} - d'\right) + \beta_1 b x f_{cd}\left(\frac{h}{2} - \beta_2 x\right) \quad \textbf{(2.46)}$$

- **Fourth point**

The failure imposed due to concrete and the lower reinforcement reaches exactly the yielding point, $\varepsilon_s = \varepsilon_{syd}$. As for the previous point, the neutral axis position is determined, N_{Ed} and M_{Rd} are determined using the equations 2.45 and 2.46 respectively.

- **Fifth point**

The failure is imposed due to concrete and the lower reinforcement reaches exactly $\varepsilon_s = 0$ then the neutral axis position is equal to the effective depth of the section. The limit axial force and bending moment id obtained from the equations 2.47 and 2.48.

$$N_{Rd} = -\beta_1 b x f_{cd} - f_{yd} A'_s \quad \textbf{(2.47)}$$

$$M_{Rd} = f_{yd} A'_s \left(\frac{h}{2} - d'\right) + \beta_1 b x f_{cd} \left(\frac{h}{2} - \beta_2 x\right) \quad \textbf{(2.48)}$$

- **Sixth point**

Now the concrete is uniformly compressed and assume the strains $\varepsilon_s = \varepsilon_c \geq \varepsilon_{c2}$. Axial force and bending moment are computed as equation 2.49 and 2.50.

$$N_{Rd} = -b h f_{cd} - f_{yd} A_s - f_{yd} A'_s \quad \textbf{(2.49)}$$

$$M_{Rd} = f_{yd} A'_s \left(\frac{h}{2} - d'\right) + f_{yd} A_s \left(\frac{h}{2} - d'\right) \quad \textbf{(2.50)}$$

Eurocode 2 provide some limitation in the steel reinforcement as describe by equations 2.51 and 2.52.

$$A_{s,min} = max = \left(\frac{0.10 N_{ED}}{f_{yd}}; 0.002 A_c\right) \quad \textbf{(2.51)}$$

$$A_{s,max} = 0.04 A_c) \quad \textbf{(2.52)}$$

With

N_{Ed}: design axial compressive force;

f_{yd}: design yield strength.

ii. Shear design

Unlike concrete girder as early explained above, shear design of column follows the same procedures however, the detailing of members prescribed by Eurocode 2 imposed a minimum diameter of 6 mm or one quarter the maximum diameter of the longitudinal bars. Equally, the maximum spacing has to be reduced by a factor 0.6 in sections within a distance equal to the larger dimension of the column cross-section above or below the beam. This maximum spacing between the transversal shear reinforcement is defined by equation 2.53.

$$S_{cl,max} = \min(20\emptyset_{l,min}; b; 400mm) \quad \textbf{(2.53)}$$

iii. Slenderness verification

Structural deformations causes additional action (second order effects) to some element. Elements like column are more likely to be affected by second order effects hence the need of slenderness verification. It consists in verifying if the slenderness of the element is below a limit value, defined by the Eurocode 2 as expressed in equation 2.54.

$$\lambda_{lim} = \frac{20ABC}{\sqrt{n}} \quad \textbf{(2.54)}$$

Where:

$A = \frac{1}{1+0.2\varphi_{ef}}$ (φ_{ef} is the effective creep ratio; $A = 0.7$ if φ_{ef} is unknown;

$B = \sqrt{1+2\omega}$ ($\omega = \frac{A_s f_{yd}}{A_c f_{cd}}$, is the mechanical reinforcement ration);

$C = 1 - r_m$ (r_m is the moment ratio, $r_m = \frac{M_{01}}{M_{02}}$;

$n = \frac{N_{ED}}{A_c f_{cd}}$ (relative normal force).

The slenderness of an element is computed using equation 2.55.

$$\lambda = \frac{l_0}{i} \quad \textbf{(2.55)}$$

Where

l_0: is the effective length of the element

$i = \frac{I}{A}$ (i, I, and A represent the gyration radius of the uncracked section, the moment of inertia and the area of the section respectively.

c. Footing design

With respect to the structural system used for the pier, the type of foundation used is pad footing. To design these elements, we follow those steps:

- Calculate the plan size of the footing using the permissible bearing pressure and the critical loading for SLS,

- Calculate the bearing pressures at ULS,

- Determine the resultant column loads,

- Determine the longitudinal from equation 2.58 and transverse bending reinforcement, like concrete girder as early explained above, shear design of footing follows the same procedures however

$$k = \frac{M_{Ed}}{bd^2 f_{ck}} \quad \textbf{(2.56)}$$

$$z = 0.9d \quad \textbf{(2.57)}$$

$$A_{s,req} = \frac{M_{Ed}}{f_{yd} z} \quad \textbf{(2.58)}$$

$k < 0.167$ no compression reinforcement required

Where

b: effective width;

d: effective depth.

2.3.3.2. Serviceability Limit State

a. Girder bridge verification

For this purpose stress limit, control cracking and deflection will be presented.

i. Stress

Frequent combination in section (2.3.2.1) will be used to verify stress in slab. In this condition, stress criterion from equation 2.59 have to be satisfied

$$\begin{cases} \sigma_c \leq 0.6 f_{ck} \\ \sigma_s \leq 0.8 f_{yk} \end{cases} \quad \textbf{(2.59)}$$

$$\text{With } \sigma_c = \frac{My}{J} \text{ and } \sigma_s = \frac{n_0 M(d-y)}{J} \quad \textbf{(2.60)}$$

Where:

σ_c is the stress in concrete;
σ_s is the stress in steel;
y is the neutral axis position;
J is the moment of inertia of the section.

ii. Cracking

Cracking shall be limited to an extent that will not impair the proper functioning or durability of the structure or cause its appearance to be unacceptable. The quasi-permanent combination will be use, because it is at long term n_L of section 2.3.2.1 will be consider.

The calculated crack width w_k from table 2.4 has to be less than the corresponding w_{max} taking from table 2.5.

Table 2.4. Maximum bar diameters Φs for crack control (EN 1991-2, 2003).

Steel stress[2] [MPa]	Maximum bar size [mm] w_k= 0,4 mm	w_k= 0,3 mm	w_k= 0,2 mm
160	40	32	25
200	32	25	16
240	20	16	12
280	16	12	8
320	12	10	6
360	10	8	5
400	8	6	4
450	6	5	-

Table 2.5. Recommended values of wmax (mmm (EN 1991-2, 2003).

Exposure Class	Reinforced members and prestressed members with unbonded tendons	Prestressed members with bonded tendons
	Quasi-permanent load combination	Frequent load combination
X0, XC1	0,4[1]	0,2
XC2, XC3, XC4	0,3	0,2[2]
[AC2] XD1, XD2, XD3, XS1, XS2, XS3 [AC2]		Decompression

Note 1: For X0, XC1 exposure classes, crack width has no influence on durability and [AC1]this limit is set to give generally acceptable appearance. In the absence [AC1] of appearance conditions this limit may be relaxed.

Note 2: For these exposure classes, in addition, decompression should be checked under the quasi-permanent combination of loads.

iii. Deflection control

Next, quasi-permanent combination will be used. The deflection has to be less than span/250 and is given by equation (2.61.a) and (2.61.b)

$$\frac{l}{d} = K\left[11 + 1{,}5\sqrt{f_{ck}}\frac{\rho_0}{\rho} + 3{,}2\sqrt{f_{ck}}\left(\frac{\rho_0}{\rho} - 1\right)^{3/2}\right] \quad \text{if } \rho \le \rho_0 \qquad \textbf{(3.61.a)}$$

$$\frac{l}{d} = K\left[11 + 1{,}5\sqrt{f_{ck}}\frac{\rho_0}{\rho - \rho'} + \frac{1}{12}\sqrt{f_{ck}}\sqrt{\frac{\rho'}{\rho_0}}\right] \quad \text{if } \rho > \rho_0 \qquad \textbf{(2.61.b)}$$

Where:

l/d is the limit span/depth;

K is the factor to take into account the different structural systems;

ρ_0 is the reference reinforcement ratio $\rho_0 = 10^{-3}\sqrt{f_{ck}}$;

ρ is the required tension reinforcement ratio at mid-span to resist the moment due to the design loads $\rho = \frac{As}{bd}$;

ρ' is the required tension compression ratio at mid-span to resist the moment due to the design loads $\rho' = \frac{As'}{bd}$.

b. Footing verification

The design criteria essentially consist of verifying that the service stress under the foundations remains below the permissible stress and that the ground settlement caused by the applied loads remains permissible.

The calculation of the permissible foundation stress is based on the results of in situ tests and the physical-mechanical characteristics of the soil.

The safety of the structure is ensured with regard to the failure of the supporting soil if the service stress due to the load applied to the soil by the structure's foundations (q_{ser}) is less than the permissible soil stress (q_{ref}).

The safety of the structure with regard to settlements (isolated or differential) is ensured if the soil settlements generated by the structure are lower than the admissible settlements.

The permissible settlements are 2.50 cm for the isolated footings, 3.75 cm for the threaded footings and 5.00 cm for the general invert.

2.3.4. Dynamic analysis

Entering in the principal part of this thesis, a presentation of the procedure that will used to perform time-history analysis will be shown.

2.3.4.1. Explosive weight and position of explosion

The explosion is that of an anti-personnel mine placed on the deck of pillar P2. The mass of the mine is fixed at 0.10 kg.

2.3.4.2. Blast load analysis

The minimum height above which the explosion can occur will be 0.10 m. The effect of the explosion decreases as the distance increases. Thus, the maximum distance of 3.75 m is

considered. The loads are blown off the deck of the P2 bridge pier. The shock wave is considered to disperse in all directions and affect all beams surrounded by the blast.

2.3.4.3. Nonlinear time-history analysis

When large loads (a blast in this case) are applied to a structure, resulting in high stresses in the range of the non-linear stress-strain relationship, a non-linear time history analysis for the dynamic study will be perform. The dynamic equilibrium equations to be solved are given by equation 2.62.

$$[M]\ddot{u}(t) + [C]\dot{u}(t) + [K]u(t) = p(t) \quad (2.62)$$

Where:

[K], [C], [M] are the stiffness matrix, the damping matrix and the diagonal mass matrix respectiely

u, $\dot{u}$, and $\ddot{u}$: are the displacement, velocity and acceleration of the structure respectively

$p(t)$ represents the applied load.

Modal-superposition is a good procedure to the non-linear problems. Therefore, this option will be use to solve the dynamic equilibrium equation in order to obtain the time-history response of the bridge against blast load.

2.4. Numerical modelling

In this section, the software used for modelling and different analyses will be presented. The software used in this thesis for different analyses starting by static analysis and finish by non-linear time history analysis is MIDAS/civil 2022.

To do static analysis of the bridge under permanent and variable loads, MIDAS/civil 2022 was used.

The different modules that will be used are presented as follows:

- **Properties:** this section is meant for definition of material and section properties of different elements (girders, slab, cross beams, transversal beams, piers and foundations)
- **Structure:** this module permits to define the geometry of the concrete bridge and affect the different sections and the corresponding material properties.
- **Boundary:** this module permits to define boundary restrains, rigid, elastic links and surface spring of the bridge.

- **Loads:** loads cases are defined here (self-weight, moving loads, element loads, nodal loads).
- **Results:** different results (displacements, stresses, moments, axial, shear forces…) can be displayed.

For dynamic analysis, the following options are used:

- **Time-history functions:** after having blast pressure distribution, a function of point force changing with time will be used. The time-history functions will be created to represent the blast loads that will act on the bridge.
- **Load cases:** depending on the number of time-history functions, the same number of load cases will be created.

For damping method, the modal damping will be chosen and assume a damping ratio of 5% because concrete bridges have really low damping ratios.

- **Display:** once analysis performance is ended, the time-history graph/results can be outcome depending on the parameters of the study.

Conclusion

The objective of this chapter was to present the steps necessary to establish the procedure for blast-induced collapse of concrete bridges. The procedure for collecting field data and material properties was illustrated. In order to perform righteous analyses, a clear methodology to obtain the loads acting on the bridge and the various loads combination was done. The software used for this thesis was shown. The design at limit state followed a clear procedure and for the case study, the standard to satisfy these limit states were explained. The blast analysis approach presentation was highlighted.

CHAPTER 3: RESULTS AND INTERPRETATION

Introdution

This section presents the results obtained from previous detailed methodology outlined in chapter 2. First, the case study which is a concrete reinforced girder bridge in Limani with the different structural elements will be shown; details on materials will be given. Then, static analysis will be performed at the ultimate limit state and checks at the service limit state to evaluate the stability of this bridge. Next, nonlinear time-history analysis would be done to effects of blast load on the bridge. Finally, some improvements will be made to increase the stability of the bridge.

3.1. General presentation of the site

This section is a brief presentation of Limani. The city will be presented geographically, climate, relief and economic conditions in order to know the different conditions that usually have a major influence on the design of structures.

3.1.1. Geographical location of the site

The collapsed structure on the Mayo Limani is located in the Mayo Sava department, Far North region, on the R0918 regional road (Kourgui (Intersection N14)) - Limani – Amchide as shows in figure 3.1.

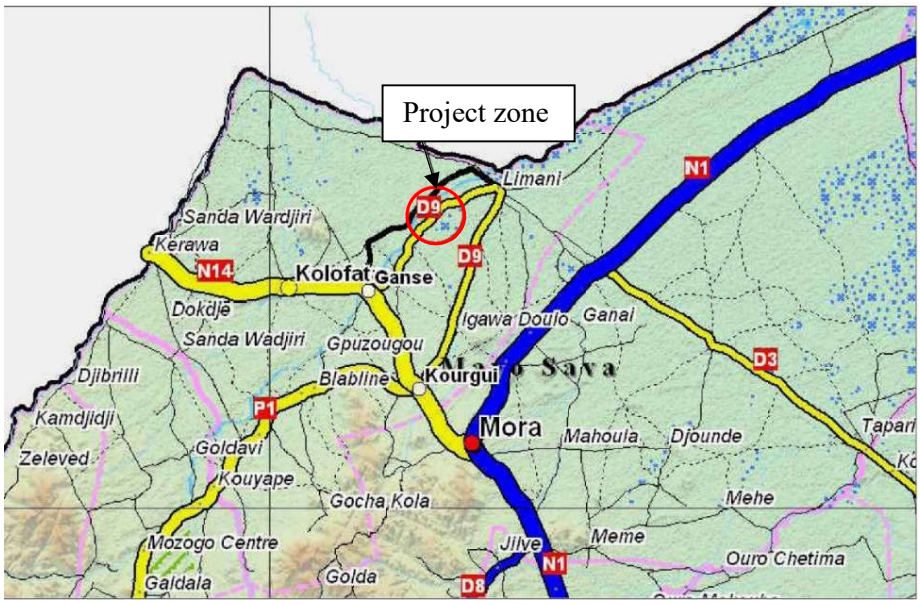

Figure 3.1. Limani bridge project location on the Cameroun map (Source: DOA,2018)

3.1.1. Relief and ground

The Sudanian savannahs, whose domain in Cameroon extends from the Adamaoua plateau in the south to the Mandara Mountains in the north, cover most of the project area. However, between the Benue and the Mandara Mountains there are Sahelian elements that make it a transitional zone towards the Sahelian domain of thorny steppes.

On the geological level, the department of Mayo-Sava and more particularly the town of Limani presents a very great diversity of soils, namely:

- Poorly developed soils: These are found at the foot of the mountains, are shallow, and are characterised by low fertility due to water erosion and its essentially stony structure. Only less demanding crops such as red millet, yellow millet and leafy vegetables succeed easily here.
- The sandy-loam soils occupy a large part of the city. They are very fertile and deep and favourable to all rainy season crops and cotton.

3.1.2. Climatic conditions

The climate of the region is distinctly Sudanese with more rainfall in the Mandara Mountains. In this climate, the dry season and the rainy season are of roughly equal duration and the average annual rainfall is in the order of 800-1000 mm. The maximum temperature (34°C) occurs at the end of the dry season, followed by a first cooling (23°C) in the wet season and a second in December (figure 3.2). The cooling of precipitation is most marked at the time of the maxima, while the lowest temperatures occur in December.

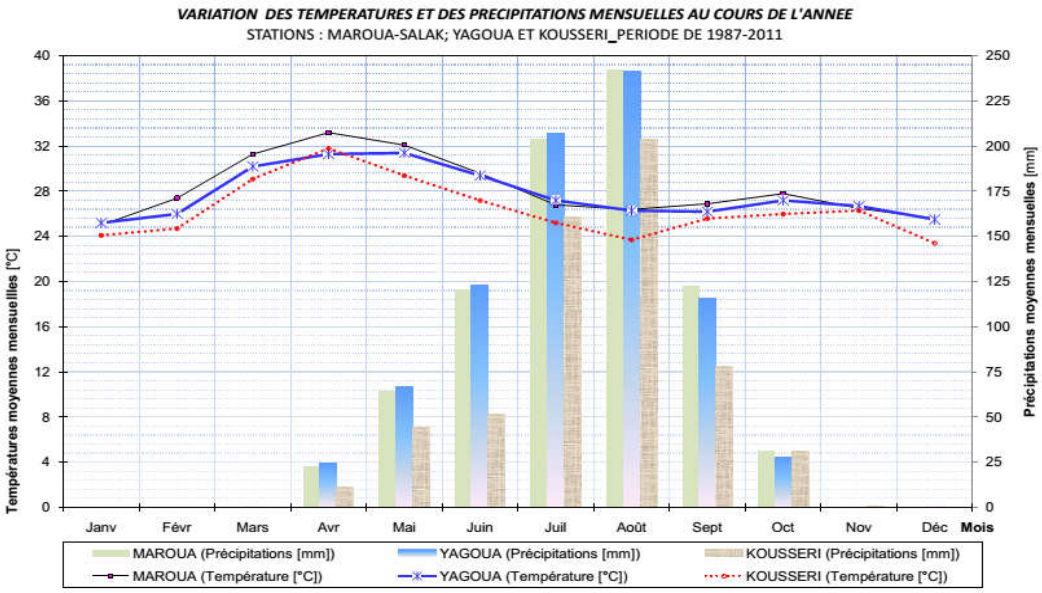

Figure 3.2. Variation in temperature and precipitation over the years (Source: DOA,2018).

3.1.3. Socio-economic aspect

Limani is a town in the Far North Region of Cameroon, on the border with Nigeria. In 2014, Limani was caught up in the Boko Haram conflict. In October 2014, Boko Haram fighters entered Limani and Amchidé as illustrated in figures 3.3 and 3.4. , another border town, killing at least thirty civilians. The Cameroonian army reported that 107 Boko Haram members were killed in the ensuing fighting. On 28 December 2014, Cameroonian troops simultaneously repelled Boko Haram raids in the towns of Limani, Amchidé, Makary, Guirvidig, Waza and Achigachia, all located in the Far North region of Cameroon.

Figure 3.3. Destruction of buildings, impact of bullets on walls and abandonment of administrations (Source: DOA,2018).

Figure 3.4. Village razed and destroyed by the clashes (Source: DOA,2018).

In 2015 this bridge was attacked by the terrorist sect BOKO HARAM. According to the chief lieutenant of the Rapid Intervention Battalion (BIR) of Limani, the bridge suffered an explosion of mines placed on this part of the bridge as shows in figure 3.5.

Figure 3.5. Damaged part of the bridge (Source: DOA,2018).

3.2. Presentation of case study

Elements which allow us to present the case study building are geometric data and statistic data.

3.2.1. Geometric data

Geometric data are essentially bridge geometry with its different cross section or views.

3.2.1.1. Bridge geometry

The characteristics of the structure built between 2008 and 2013 are presented in the table 3.1.

Table 3.1. The characteristics of the structure.

Length of the bridge:	120 ml
Number of spans:	12 identical and independent spans of 10 m
Number of lanes:	One (01) lane
Width of the bridge:	5.60 ml (including the footbridges on both sides of the structure which serve as pavements for the population)
Width of the roadway:	1 x 3.50 ml (3.50 ml)
Width of pavement:	2 x 0.80 ml (0.80 ml)
Type of bridge :	Reinforced concrete bridge, Reinforced concrete girders and deck
Thickness of the slab:	25 cm
Type of foundation:	Combined footing
Ground surface of the footing	4.30 x 3.00, i.e. 12.9 m²
Height of the footing	0.70 m
Cross-section of the sill before the pile shaft	0.60 x 0.60 m
Height of the pile shafts P2	7.34 m
Height of the pile shafts P1,P3,…,P9	5.34 m
Cross-section of the Pier	0.50 x 1.00 m
Cross-section of the pier cap	0.60 x 0.60 m
Height of the I girder	0.65 m

On this view, the bridge length is along the X direction. Y direction is for transversal width of bridge and Z axis is for height (figure 3.6).

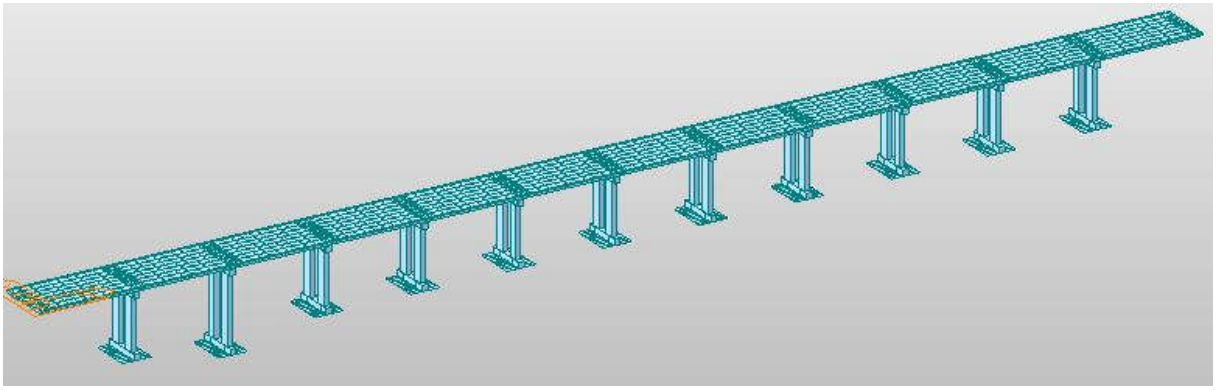

Figure 3.6. Longitudinal view of bridge model.

The total width of the bridge is 5.60m and it is a single lane road with a width of 3.5 m. and 2 pedestrian sidewalks each of width 1,05m. The figure 3.7 illustrates the transversal section of the bridge deck showing the total width of 5.60 m.

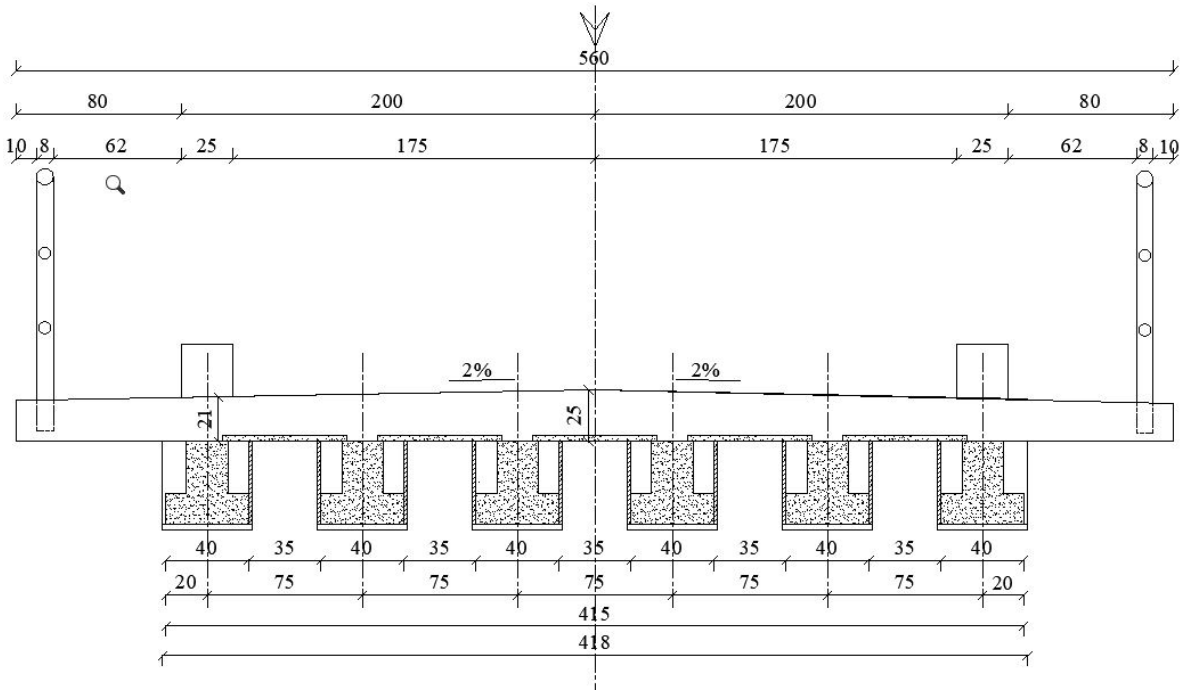

Figure 3.7. Transversal section of the bridge deck (Source: DOA,2018).

.

3.2.2. Statistic data

Statistic data will deal with presentation of data link to characteristics of concrete.

a. Characteristics of material

The concrete bridge belongs to C30/37 resistance class with normal setting (N). For steel reinforcement, Fe400 was considered. The principal characteristics of concrete and steel reinforcement used in this analysis are reported in tables 3.2 and 3.3 respectively.

Table 3.2. Characteristics of concrete.

Designation	Values	Units
Characteristic cubic Compressive strength of concrete f_{ck}	30.00	N/mm^2
Characteristic cylinder Compressive strength of concrete f_{ck}	37.00	N/mm^2
Mean tensile strength of concrete f_{ctm}	2.90	N/mm^2
Designed compressive strength of concrete f_{cd}	17.00	N/mm^2
Concrete elastic modulus E_{cm}	33000.00	N/mm^2

Table 3.3. Characteristics of steel reinforcement.

Designation	Values	Units
Characteristic yield strength of steel f_{yk}	400	N/mm^2
Design yield strength of steel f_{yd}	347.83	N/mm^2
Steel Elastic modulus E_s	200000.00	N/mm^2

Plastic properties for C30/37 and Fe 400 are defined following Von Mises yield criterion .Plastic materials are defined because of dynamic nonlinear analysis that will be done further.

Soil structure interaction is considered in this work with modulus of subgrade reaction $K_s = 17105.6\ kN/m^3$, the characteristics of the soil at SLS are in the table 3.4

Table 3.4. Characteristics of soil.

Pilars/ footing	Footing section, AxB (mxm)	Anchorage depth / TN, (m)	Soil stress SLS (kPa)
P11,P10, P9, P8	4.30 x 3.00	3.00	213.2

P7,P6, P5, P4	4.30 x 3.00	3.00	304.6
P3, P1	4.30 x 3.00	3.00	388.2
P2	4.30 x 3.00	4.50	319.6
P2	4.30 x 3.00	3.00	142.0

b. Steel reinforcement

The distribution of reinforcing bars in slab is presented in figure 3.8.

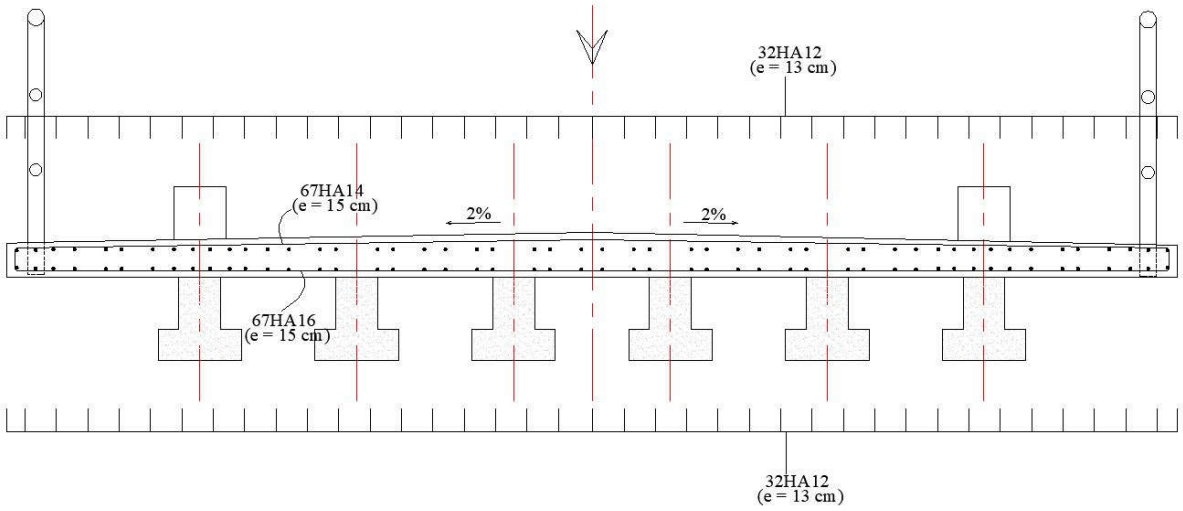

Figure 3.8. Steel reinforcement in slab (Source: DOA,2018).

c. Exposure classes and concrete cover

The design working life is of bridge is 100 years. Requirements on concrete cover are establishing based on the link between the environmental conditions and the protection of reinforcement. Exposure classes of concrete are the following:

- For top of slab: XC3 due to moderate humidity
- For slab bottom: XC4 (concrete surfaces subject to water contact) and XS3 (parts of marine structures)
- For concrete cast-in place: XC4 and XS1 (exposed to airborne salt but not in direct contact with sea water).

The basic data for the concrete cover is detailed in table 3.5.

Table 3.5. Concrete cover calculation.

Exposure class	**Bond type**	**$C_{min,b}$ (mm)**	**$C_{min,dur}$ (mm)**	

XC3	Reinforcing bars	20	30	10
XC4	Reinforcing bars	25	40	10
XS1	Reinforcing bars	25	45	10

$\mathbf{C_{min}}$ =max ($\mathbf{C_{min,b}}$; $\mathbf{C_{min,dur}}$; 10 mm)

Concrete cover will be considered as 40mm for superstructure and 50mm for substructure.

3.3. Structural analysis of bridge

3.3.1. Loads computation

The values of the permanent and variable loads acting on the bridge are determined.

3.3.1.1. Self-weight of structural elements (g_1)

Table 3.5 shows a self-weight estimation concerning structural element concrete slab and ($g_{1,cs}$) and structural element concrete girder $g_{1,gir}$, both expressed as distributive loads show in table 3.6.

Table 3.6. Self-weight of structural elements.

Loads	**Weight density [kN/m³]**	***g₁* [kN/m]**
$g_{1,cs}$	25	37.75
$g_{1,gir}$	25	4

3.3.1.2. Self-weight of non-structural elements (g_2)

Self-weights of non-structural elements are summarised in table 3.7.

Table 3.7. Self-weight of structural elements.

Elements	**Number**	**Weight density [kN/m³]**	**Width/ diameter [m]**	**Thickness/ height [m]**	**Characteristic value [kN/m]**
Left footway					
Safety barrier	1	/	/	/	0,65

Footway concrete	1	25	1,05	0,25	6.5625
Low wall	1	25	0.2	0.25	1.25
Right footway					
Safety barrier	1	/	/	/	0,65
Footway concrete	1	25	1,05	0,25	6.5625
Low wall	1	25	0.2	0.25	1.25
Roadway					
Waterproofing layer	1	22	5.6	0,03	3.696
Asphalt layer	1	22	5.6	0,07	8.624

3.3.1.3. Shrinkage

On figure 3.9, at time t=∞, $\rho = 2.1163$.

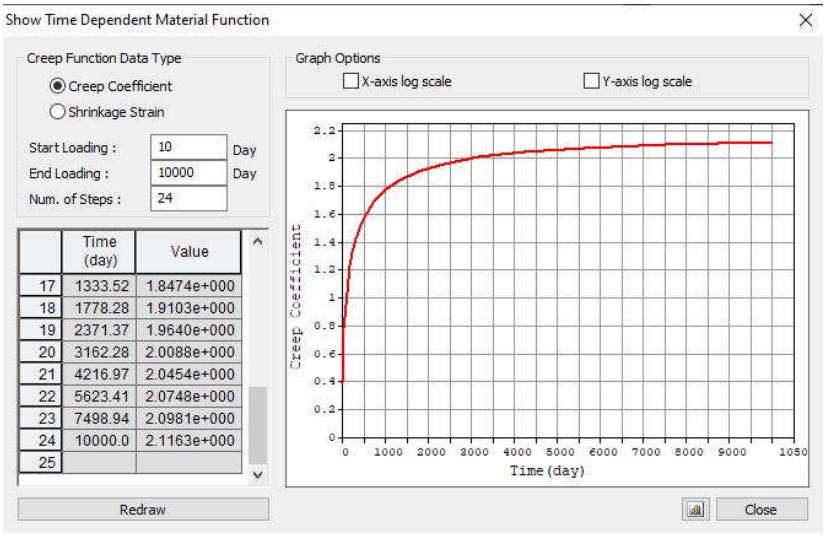

Figure 3.9. Creep coefficient graph.

Looking at graph on figure 3.10, at time t=∞, $\varepsilon_{cs}(\infty) = -2.9744E-04$

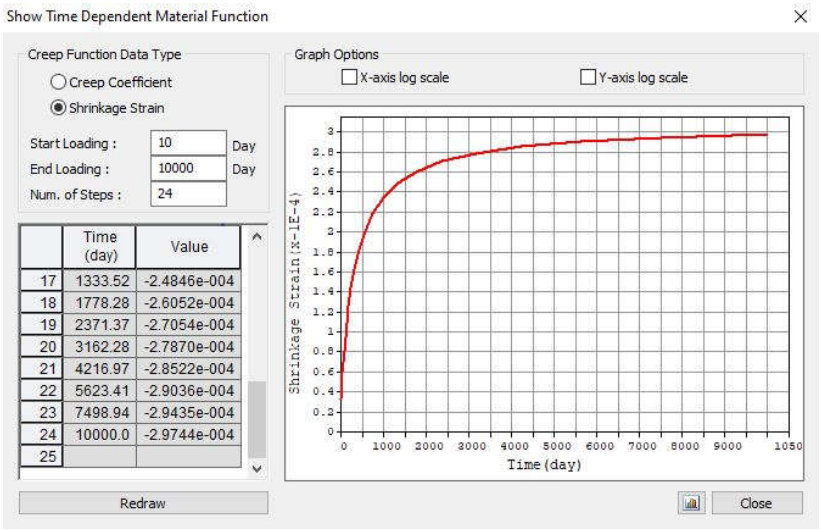

Figure 3.10. Shrinkage strain graph.

Values of different coefficients and axial force value obtained for shrinkage figured in table 3.8.

Table 3.8. Shrinkage computation.

Designation	**Values**	**Units**
Total shrinkage force $N_{c,r\infty}$	4021.7	kN
Shrinkage force per effective section N_{beam}	670.3	kN

3.3.1.4. Live loads

For traffic distribution, load values of traffic are reported in table 3.9.

Table 3.9. Load values for group 1a.

	Lane 1	**Residual area**	**Footway**
Width of the notional lane [m]	3	0,5	1,05
Uniformly distributed load UDL [kN/m²]	9	2,5	3
Concentrated load TS [kN] (value of single axle)	300	0	0

3.3.1.5. Wind load

This project faces a terrain of category II (z_0=0.05 m and z_{min}=2 m). The reference speed was set at $V_{b,0}$ = 20 m/s (obtained from project notes Zone 1). The values of coefficients at height z=5 m used in this process are reported in table 3.10.

Table 3.10. Coefficients of wind.

Coefficients	**Values**
Roughness coefficient $c_r(z)$	0.875
Orography coefficient $c_o(z)$	1
Turbulence factor k_l	1
Directional factor c_{dir}	1
Season factor c_{season}	1

For wind force applied in y direction, the computed value figure in table 3.11.

Table 3.11. Wind force computation.

Designation	**Values**	**Units**
Basic wind velocity v_b	20	m/s
Mean velocity v_m	20	m/s
Turbulence intensity $I_v(z)$	0.217	/
Peak velocity pressure $q_p(z)$	583.62	N/m^2
Total depth d_{tot}	4.65	m
Force coefficient c_f	2.15	/
Wind force $F_{w,y}$	6.51	kN/m

3.3.1.6. Temperature load

Table 3.12 presents temperature load calculation.

Table 3.12. Temperature force computation.

Designation	**Values**	**Units**
Slab area A_c	1.4	m^2
Thermal coefficient ε	1.2E-05	/
Total temperature load T_k	5516.54	kN

Temperature force per effective section	919.42	kN

3.3.2. Verification at Ultimate Limit State

At the ultimate limit state, the verifications of the beams, piers and footings will be performed.

3.3.2.1. Verifications of girder

a. Calculation of steel reinforcement

The steel reinforcement at span, support and abutment are shows in table 3.13.

Table 3.13. Calculation of steel reinforcement.

Location	M_{Ed} **(kNm)**	$A_{s,req}$ **(mm²)**	**Diameter of reinforcement used**	$A_{s,pro}$ **(mm²)**	M_{Rd} **(kNm)**
Span	534.41	2810	12Ø20	3769	699.66
Support	403.31	2551	14Ø20	4398	908.75
Abutment	730.31	3840	14Ø20	4398	908.75

b. Transverse reinforcement

The designed shear value at support is given by V_{Ed} = 374 kN at support ,to resist to this, the shear reinforcement provide is Ø8 used with spacing of 15 cm at supports and with spacing of 30 cm at mid span.

c. Disposition of reinforcement

The arrangement of steel reinforcement of girder are shows in figure 3.11, 3.12 and 3.13.

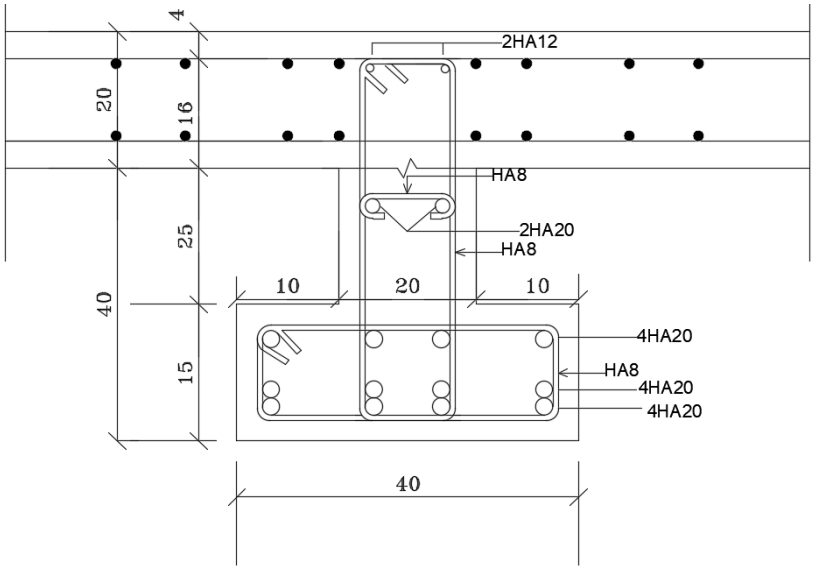

Figure 3.11. Cross section of girder at mid span.

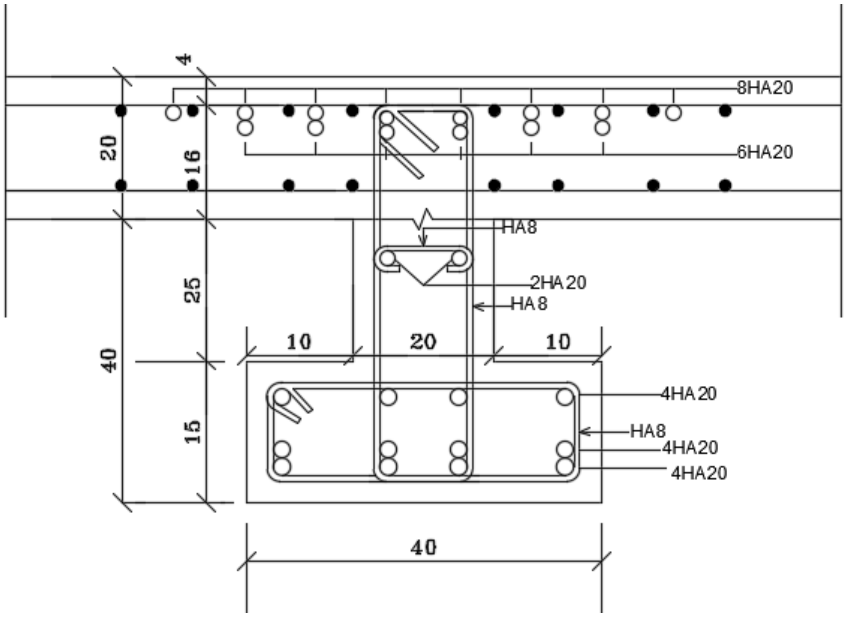

Figure 3.12. Cross section of girder at pier and support.

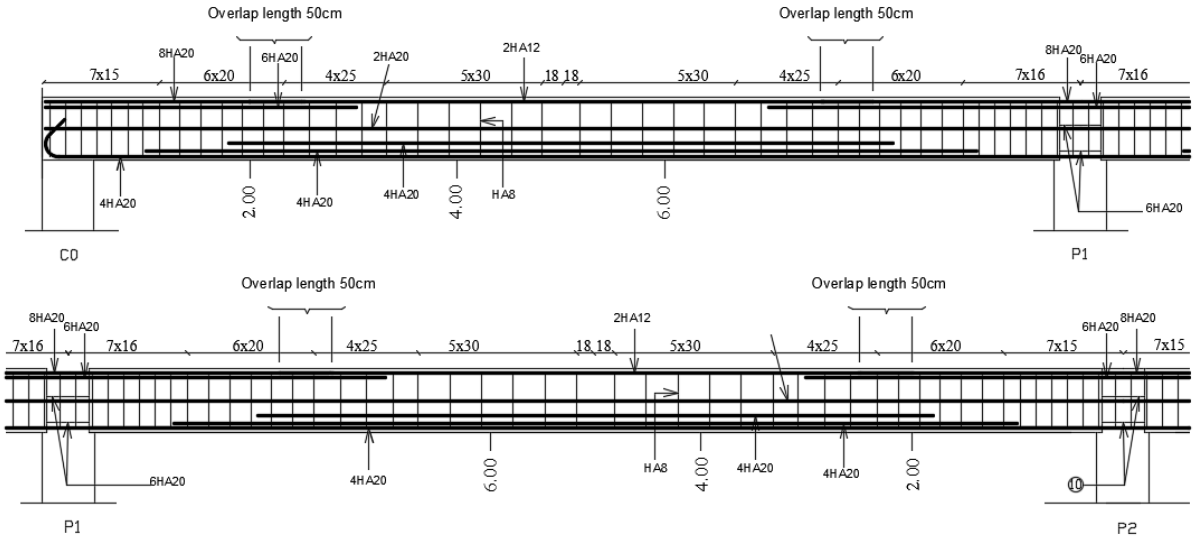

Figure 3.13. Longitudinal reinforcement of designed girder.

3.3.2.2. Verifications of piers

a. Bending moment and axial force verification

The verification of the axial loads and the bending moment is done through the interaction diagram as presented in section 2.2.4. Complying with Eurocode 2 as described in the same section, 1000 $mm^2 \leq As \leq 20000\ mm^2$. The column will be provided with 12Ø20 (1357 mm^2). The cross section of column is shown in figure 3.14.

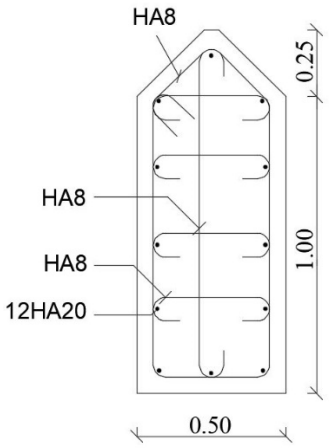

Figure 3.14. Column cross section.

Here, the main interest will be to design the pier element with maximum axial, shear forces and bending moment. The solicitations obtained are given in table 3.14 and the verifications in table 3.15.

Table 3.14. Solicitations of the column.

N_{Ed}(kN)	M_{Edy}(kNm)	M_{Edz}(kNm)	M_{Ed}(kNm)
1313.35	-131.98	-20.305	133.536

Table 3.15. Axial forces and moments resistance check.

Concentric Max. Axial Load	N_{Rdmax} = 9747.19 kN	
Axial Load Ratio	N_{Ed}/N_{Rd} = 1313.35 / 6042.79	= 0.217 < 1.000 **OK**
Moment Ratio	M_{Edy}/M_{Rdy} = -131.98 / 610.248	= 0.216 < 1.000 **OK**
	M_{Edz}/M_{Rdz} = -20.305 / 89.7470	= 0.226 < 1.000 **OK**
	M_{Ed}/M_{Rd} = 133.536 / 616.812	= 0.216 < 1.000 **OK**

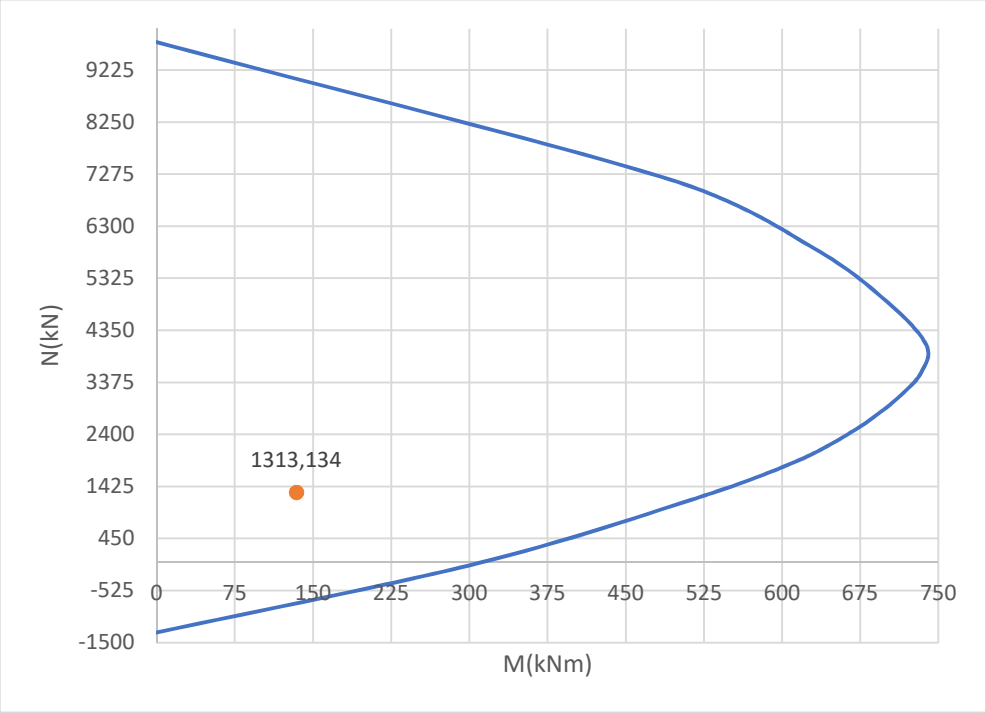

Figure 3.15. N-M Interaction Diagram.

For all piers, the M-N (bending moment-axial force) values lies within the interaction diagrams. Hence verified in figure 3.15.

- **Shear verification**

From the shear solicitations displayed in the previous part and following the procedure explained in section 2.3.3.1, it is observed that the shear resistance of the section without shear reinforcement is greater than the maximum shear solicitation on the column. Hence for Ø8 used, the maximum spacing of the transverse reinforcement is:

$$S_{cs,max} = min(400; 500; 400) = 400\ mm$$

Hence, a spacing of 240 mm will be applied.

- **Slenderness verification**

Following the steps in 2.3.3.1, the parameters to compute are displayed in table 3.16.

Table 3.16. Parameters for slenderness verification.

n	ω	A	B	C	λ_{lim}	λ
0.15	0.15	0.7	1.14	1.89	77.19	48.84

.

From the table 3.15 $\lambda < \lambda_{lim}$, so the slenderness of the column is verified.

3.3.2.3. Verifications of footing

The steel reinforcement of footings are calculated in table 3.17 and 3.18.

Table 3.17. Flexural design in longitudinal direction.

Location	M_{Ed} **(kNm)**	$A_{s,req}$ **(mm²)**	**Diameter of reinforcement**	$A_{s,pro}$ **(mm²)**
Long top	109.20	547	16Ø8	805
Long bot	533.60	2752	16Ø14	4423

Table 3.18. Flexural design in tranverse direction.

Location	M_{Ed} **(kNm/m)**	$A_{s,req}$ **(mm²)**	**Diameter of reinforcement**	$A_{s,pro}$ **(mm²)**
Long top	/	/	22Ø8	1105
Long bot	338.63	2752	22Ø16	2463

3.3.2.4. Disposition of reinforcement

Detailing checks should be carried out to ensure compliance with code specification. The figures 3.16, 3.17 and 3.18 shows the top view and cross sections the foundations.

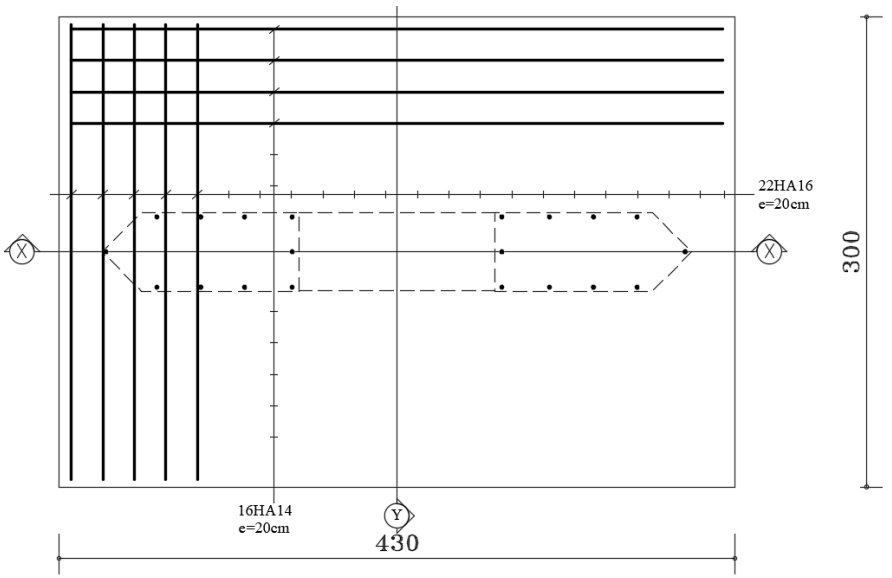

Figure 3.16 Plan view of footing.

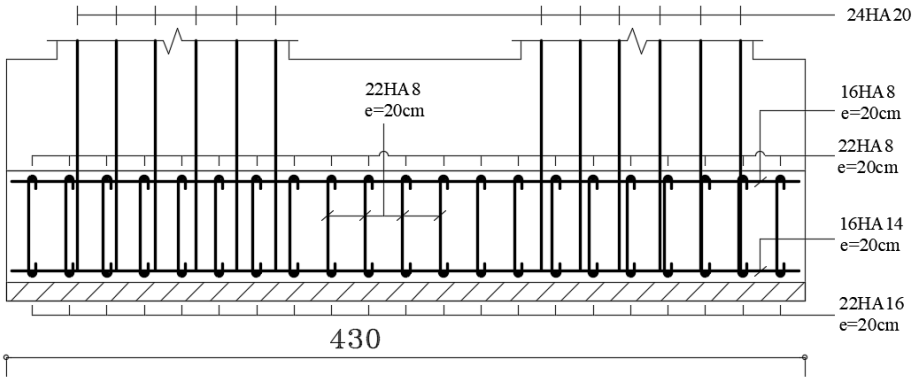

Figure 3.17. Cross section X-X

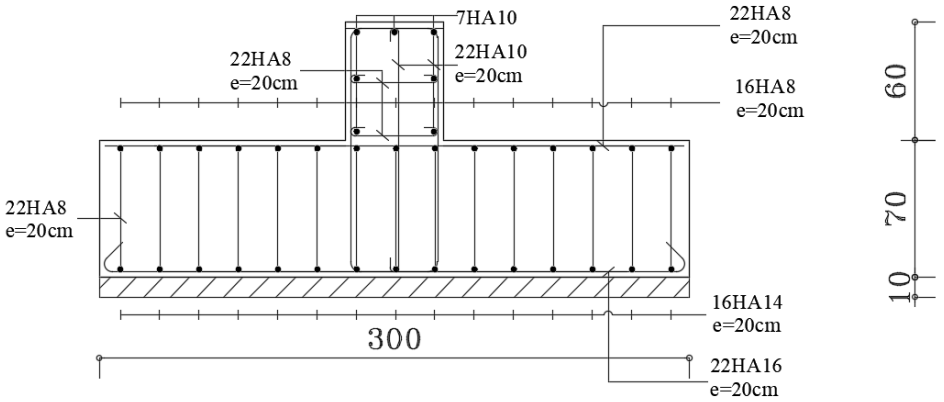

Figure 3.18. Cross section Y-Y

3.3.3. Serviceability Limit State

At the SLS, the verifications of the beams, piers and footings will be performed.

3.3.3.1. Verifications and detailling checks of slab

Slab stresses, cracks, and deflection will be checked at serviceability limit state (SLS) conditions as shown in table 3.19.

Table 3.19. Verifications required for Slab.

		Conditions	Verifications
SLS verifications	Deflection (l/d)	$(l/d)_{allowable} > (l/d)_{actual}$	$(l/d)_{allowable}$ = 90.90 mm $> (l/d)_{actual}$ = 47.62 mm **OK**
	Stress (σ)	$\sigma_c < 0.6 f_{ck}$ $\sigma_s < 0.8 f_{ck}$	$\sigma_c = 5.89 < 18(MPa)$ $\sigma_s = 169.61 < 320(MPa)$ **OK**
	Cracking	$\sigma_s = 151.46\ MPa$ Read from table with a crack width of 0.3 mm:	Max bar size = 32 mm **OK**

3.3.3.1. Verifications and detailling checks of girder

Girder stresses, cracks, and deflection will be checked at serviceability limit state (SLS) conditions as shown in table 3.20.

Table 3.20. Verifications required for girder.

		Conditions	Verifications
SLS verifications	Deflection (l/d)	$(l/d)_{allowable} > (l/d)_{actual}$	$(l/d)_{allowable}$ = 39.52 mm $> (l/d)_{actual}$ = 17.29 mm **OK**
	Stress (σ)	$\sigma_c < 0.6 f_{ck}$ $\sigma_s < 0.8 f_{ck}$	$\sigma_c = 12.25 < 18(MPa)$ $\sigma_s = 190.1 < 320(MPa)$ **OK**
	Cracking	$\sigma_s = 146.45\ MPa$ Read from table with a crack width of 0.3 mm:	Max bar size = 32 mm **OK**

3.3.3.2. Verification of the stability of foundation footings

The above mentioned stresses are calculated for a soil settlement of 2.54 cm or less. The calculation of the permissible stress is made using the sounding carried out in the vicinity of the open footing or the one close to it in the case of a sounding with early rejection. Table 3.21 show the stability of footing in SLS combination.

Table 3.21. Stability of footing.

Pilars/ footing	Footing section, AxB (mxm)	Anchorage depth / TN, (m)	Transmitted pressure at SLS (kPa)	Soil stress SLS (kPa)	Opinion on stability
P11,P10, P9, P8	4.30 x 3.00	3.00	186.07	213.2	Stability verified
P7,P6, P5, P4	4.30 x 3.00	3.00	186.07	304.6	Stability verified
P3, P1	4.30 x 3.00	3.00	186.07	388.2	Stability verified
P2	4.30 x 3.00	4.50	186.07	319.6	Stability verified

As the footing of pier 2 is not founded at the same level as the others, the differential settlement observed is $\Delta_S = 2.50 - 2.06 = 0.44\ cm$. This differential settlement is admissible.

3.4. Results of blast analysis

The non-linear modal analysis of the time history is performed.

3.4.1. Blast functions

From section 2.3.4, the different parameters of the blast wave are calculated. Table 3.22 shows the overall blast wave parameters for the top face of the bridge, gave a charge weight of 0.10 kg. Figure 3.19 illustrates the position of blast load on the deck.

Table 3.22. Blast load parameters relative to the top face of the bridge.

Girder	R(m)	$Z\ (m/kg^{(1/3)})$	Pso (kN/m²)	ta (ms)	to (ms)	P (kN)
Girder 01	0,10	0,215	166301,29	0,02	0,12	205382.10
Girder 02	0,75	1,616	459,85	0,46	0,93	327,64
Girder 03	1,50	3,232	82,55	1,86	1,39	58,81
Girder 04	2,25	4,847	36,84	3,71	1,76	26,25
Girder 05	3.00	6,463	22,85	5,97	1,86	16,28
Girder 06	3,75	8,079	16,51	7,97	2,55	11,76

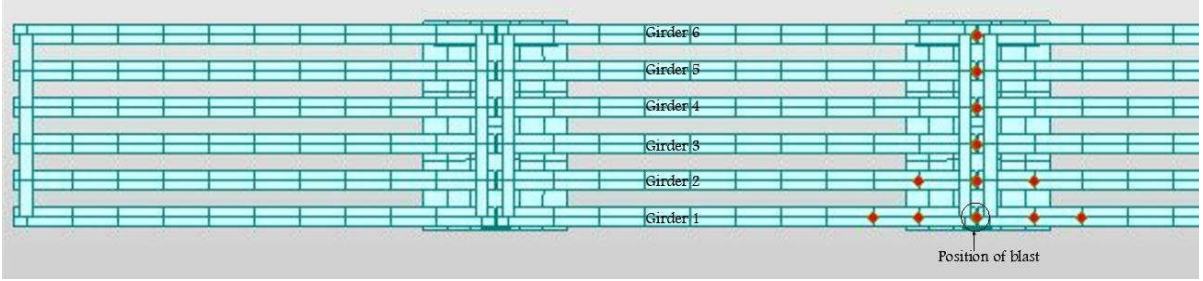

Figure 3.19. Position of blast load.

3.4.2. Interpretation of results

3.4.2.1. Moment and shear capacities of bridge

From the Midas civil program general postprocessing output, the applied moments and shear forces on the critical sections of the bridge components were determined, and compared with their respective capacities to assess their performance, the blast load case is considered for an explosion at 0.1 m above the deck of pillar P2 of bridge. The results are shown in table 3.23. The performance was evaluated by comparing the applied moments and shear forces with the respective capacities of the components. The applied blast load exceeds bridge component do not excess the capacity, then the component under consideration can not be considered to have reached the failure stage. The beam stress after blast load is showed by figure 3.20.

Table 3.23. Member status for blast load.

	Member	Bending moment (kNm)	Shear /axial*(kN)	Strutural failure
Span 2	Girder 1	60,9	-330,2	No
	Girder 2	59,7	-92.0	No
	Girder 3	-1,7	4,4	No
	Girder 4	-2.0	1,9	No
	Girder 5	-3,6	5,1	No
	Girder 6	-8.0	-1,1	No
	Girder 1	67,7	311,6	No
Span 3	Girder 2	6,1	104,7	No
	Girder 3	-3,6	-2,4	No
	Girder 4	-2,1	-2,32	No
	Girder 5	-3,6	-6,52	No
	Girder 6	-1,6	1,6	No
	Pier Cap	-235,1	-313,8	No
	Column 1	-161.5	-1965.6	No
	Column 2	-92.5	645.1	No

* Axial loads for columns only

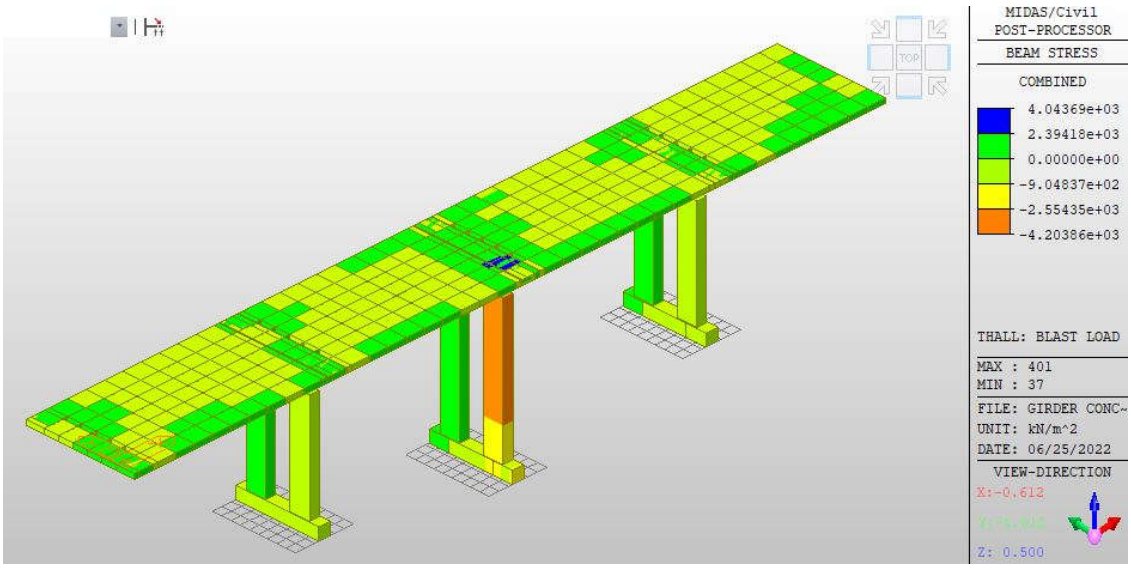

Figure 3.20. Beam stress for blast load.

3.4.2.2. Stability of footing

As the footing of pier P2 is not found at the same level as the others. From table 3.24, the pier P2 is not stable after the blast. the differential settlement is $\Delta_S = 2.50 - 3.01 = -0.51\ cm$. This differential settlement is not admissible. Figure 3.21 shows the soil pressusre due to blast load at footing.

Table 3.24. Stability of footing after the blast.

Piers/ footing	Footing section, AxB (mxm)	Anchorage depth / TN, (m)	Transmitted pressure at SLS (kPa)	Soil stress SLS (kPa)	Opinion on stability
P11,P10, P9, P8	4.30 x 3.00	3.00	186.07	213.2	Stability verified
P7,P6, P5, P4	4.30 x 3.00	3.00	186.07	304.6	Stability verified
P3, P1	4.30 x 3.00	3.00	198.72	388.2	Stability verified
P2	4.30 x 3.00	4.50	384.11	319.6	Stability not verified

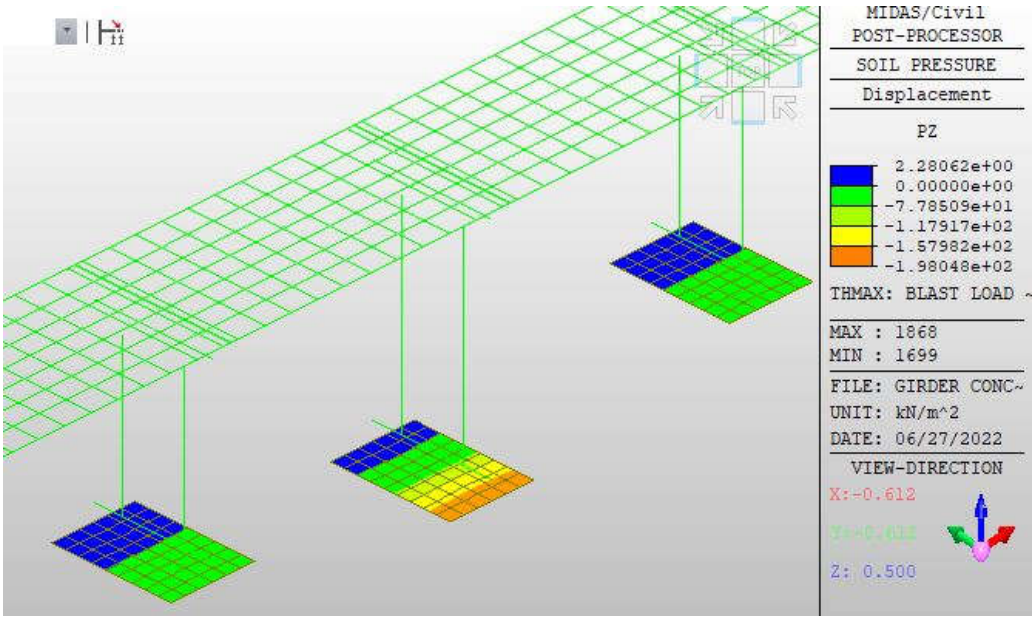

Figure 3.21. Soil pressusre due to blast load at footing.

This analysis allows us to conclude that the collapse of the bridge is due to external forces or loads not taken into account in the design. Figure 3.22 shows the deformed shape of bridge after the blast load.

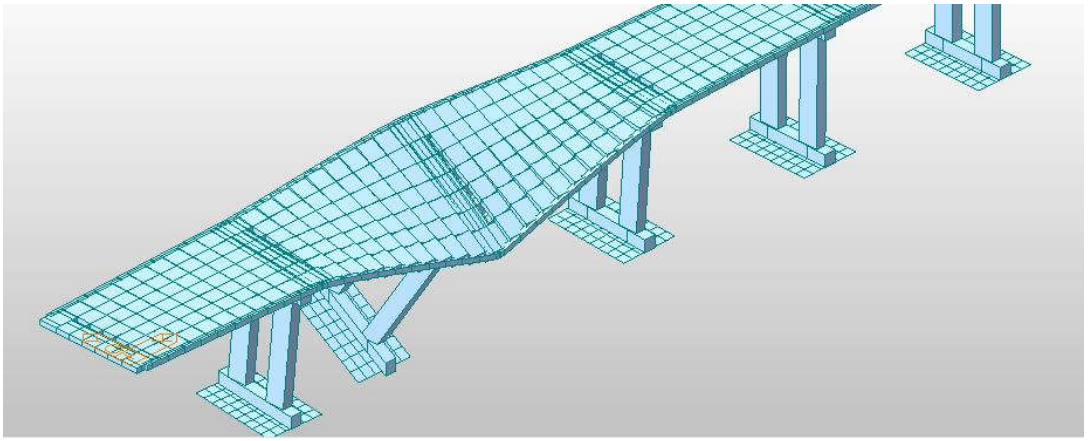

Figure 3.22. The deformed shape of bridge after the blast load.

3.5. Some possible improvements

Solutions such as the straightening beam, increased foundation dimensions and raft foundations are designed in this section.

3.5.1. Straightening beam

The supports P1 to P9 are connected by a 0.6 x 0.7 m straightening beam, anchored at 8 m at the same level as the footing of the support P1 and having the characteristics listed in the table 3.24.

Table 3.25. Straightebing beam.

Designation	**Straightening beam**
Total weight of one support (kN)	2355.7
Number of supports	P2
Total load at footing (kN)	2355.7
Choice of footing sections (m x m)	4.30 x 3.00
Total transmitted pressure at SLS σ_{adm} (kPa)	206.8
Permissible soil stress at -9.5m depth/red line $\sigma_{sol,SLS}$ (kPa)	319.6
Verification of the stability $\sigma_{sol,SLS}/\sigma_{adm} > 1$	$319.6/206.8 = 1.54 > 1$ **OK**

3.5.2. Design the foundation of pier P2

The P2 support rests on a 5.0 x 3.5 m footing anchored at 9.5m at the same depth as the P2 support footing and having the characteristics listed in the table 3.25.

Table 3.26. Foundation P2.

Designation	**Foundation pier P2**
Total weight of one support (kN)	2355.7
Number of supports	1
Total load at footing (kN)	2355.7
Choice of footing sections (m x m)	5 x 3.5
Total transmitted pressure at SLS σ_{adm} (kPa)	285.7
Permissible soil stress at -9.5m depth/red line $\sigma_{sol,SLS}$ (kPa)	319.6
Verification of the stability $\sigma_{sol,SLS}/\sigma_{adm} > 1$	$319.6/287.7 = 1.11 > 1$ **OK**

3.5.3. Raft foundation

Taking into account the checks on the stability of the foundations, the supports (P1, P2, and P3) will rest on a portion of invert on 30 cm of crushed gravel anchored at the same level as the footings of the other supports and having the characteristics listed in the table 3.26.

Table 3.27. Portion of raft.

Designation	**Portion of raft**
Total weight of one support (kN)	2355.7
Number of supports	3(P1, P2, P3)
Total load at footing (kN)	7067.1
Choice of footing sections (m x m)	23.5 x 4.30
Total transmitted pressure at SLS σ_{adm}(kPa)	70

Permissible soil stress at -8m depth/red line $\sigma_{sol,SLS}$ (kPa)	142.0
Verification of the stability $\sigma_{sol,SLS}/\sigma_{adm} > 1$	$142/70 = 2.03 > 1$ **OK**

Conclusion

The key point of this chapter was to show the results of dynamic analysis investigated on concrete bridge. It has started with presentation of details on the case study. After a static analysis was made to ensure bridge stability. Followed by dynamic analysis, the response of girders, piers caps and piers elements has been studied under high impact loading. The results show that when the blast occurred, stresses remain in a good range. The overall results show that the foundation of the P2 pillar was heavily damaged by the explosive load and that the collapse of the structure will occur with an uncoupling of this support. The intensity of the blast loads depends on several parameters such as the weight of the load, the safety distance and the angle of incidence. Some improvements that could be apply have been done such that the structure can withstand better the blast loads.

GENERAL CONCLUSION

Having reached the end of this study entitled "Collapse of bridges from the twentieth century to today: causes and improvements", it is recalled that the aim of the work was to evaluate the partial collapse of a concrete bridge, caused by the instability of a pier under the effect of blast loads with a case study on Limani bridge in Far North region of Cameroun. In order to achieve this objective, the first chapter reviewed the causes of bridge collapse, the mechanisms of bridge collapse due to blast, the consequences of bridge failures as well as the definition of the blast load. Then, the second chapter presented the methodology to be used and the third chapter was based on the presentation and interpretation of the results. The pressure-time function of the blast loads was obtained using an Excel sheet. The structure was modeled in the MIDAS/civil 2022 software, where the stresses were obtained and a static analysis carried out. After ensuring the stability of the structure, the blast analysis was performed.

The results of the analysis revealed that the blast created high stresses in the foundations. When blast occurs, the stresses do not cross the yield limit for structural elements, the structure therefore resists the explosion well but, due to the high loads, but causes an instability of the foundations with a ratio between permissible soil stresses at -9.5 m depth respect to the red line and the total transmitted pressure at SLS 0.83 less than 1 on the pier P2. To avoid this instability, the straightening beam, increased foundation dimensions of the pier P2 and raft foundations of the piers P1, P2 and P3 are used and given respectively for the a ratio between permissible soil stress at -9.5 m,-9.5 m and -8 m depth respect to the red line and the total transmitted pressure at SLS 1.54, 1.11 and 2.03 all higher than 1.

The subject dealt with is very vast and it was necessary to limit the field of research for this work. However, this work cannot be free from imperfections due to the non-performance of certain analysis such as the impact of the blast on the substructure during the blast analysis and the effect of the temperature released on the bridge structure. In order to improve this work, the following suggestions can be made for future research's:

- An optimization of the bridge in order to resist extreme event such as blast loading;
- Effect of temperature released during blast on bridge;
- Effect of blast at mid-span.

BIBLIOGRAPHY

AASHTO. (2012). *AASHTO LRFD Bridge Design Specifications, 6th Edition - June 2012 Errata* (Vol. 20001, Issue 202).

Bai, Y., Asce, M., Burkett, W. R., & Nash, P. T. (2006). *Rapid Bridge Replacement under Emergency Situation : Case Study*.

Biezma, M. V., & Schanack, F. (2007a). *Biezma2007.Pdf*. *October*, 398–405.

Biezma, M. V., & Schanack, F. (2007b). Collapse of Steel Bridges. *Journal of Performance of Constructed Facilities*, *21*(5), 398–405. https://doi.org/10.1061/(asce)0887-3828(2007)21:5(398)

Chen, Q., Wang, L., & Zhao, H. (2009). Hydrodynamic Investigation of Coastal Bridge Collapse during Hurricane Katrina. *Journal of Hydraulic Engineering*, *135*(3), 175–186. https://doi.org/10.1061/(asce)0733-9429(2009)135:3(175)

Cheng, J., Jiang, J. J., Xiao, R. C., & Xiang, H. F. (2002). Advanced aerostatic stability analysis of cable-stayed bridges using finite-element method. *Computers and Structures*, *80*(13), 1145–1158. https://doi.org/10.1016/S0045-7949(02)00079-2

Choudhury, J., & Hasnat, A. (2015). Bridge collapses around the world: Causes and mechanisms. *IABSE-JSCE Joint Conference on Advances in Bridge Engineering-III*, *August*, 651. https://www.researchgate.net/publication/281280663_Bridge_collapses_around_the_world_Causes_and_mechanisms

Cook, W., & Barr, P. J. (2017). Observations and Trends among Collapsed Bridges in New York State. *Journal of Performance of Constructed Facilities*, *31*(4), 04017011. https://doi.org/10.1061/(asce)cf.1943-5509.0000996

De Matteis, G., Zizi, M., & Del Prete, A. (2019). Structural features of typical Italian bridges built in the ‘50s: four case studies in the province of Caserta. *Proceedings of the 7th Structural Engineers World Congress 2019*, *May*.

Deng, L., Wang, W., & Yu, Y. (2016). State-of-the-Art Review on the Causes and Mechanisms of Bridge Collapse. *Journal of Performance of Constructed Facilities*, *30*(2), 04015005. https://doi.org/10.1061/(asce)cf.1943-5509.0000731

EN 1991-1-4 (Vol. 1, Issue 2005). (2011).

EN 1991-2 (Vol. 1, Issue 2005). (2003).

Fiorillo, G., & Ghosn, M. (2017). Fragility analysis of bridges due to overweight traffic load ABSTRACT. *Structure and Infrastructure Engineering*, *2479*(October), 1–15. https://doi.org/10.1080/15732479.2017.1380675

Garg, R. K., Chandra, S., & Kumar, A. (2020). Analysis of bridge failures in India from 1977 to 2017. *Structure and Infrastructure Engineering*, *18*(3), 295–312. https://doi.org/10.1080/15732479.2020.1832539

Garlock, M., Paya-Zaforteza, I., Kodur, V., & Gu, L. (2012). Fire hazard in bridges: Review, assessment and repair strategies. *Engineering Structures*, *35*, 89–98. https://doi.org/10.1016/j.engstruct.2011.11.002

Ghali, B. A., & Tadros, G. (1997). *Bridge progressive collapse vulnerability*. *February*, 227–231.

Hao, H., & Tang, E. K. C. (2010). Numerical simulation of a cable-stayed bridge response to blast loads, Part II: Damage prediction and FRP strengthening. *Engineering Structures*, *32*(10), 3193–3205. https://doi.org/10.1016/j.engstruct.2010.06.006

Hong, J.-H., Chiew, Y.-M., Lu, J.-Y., Lai, J.-S., & Lin, Y.-B. (2012). Houfeng Bridge Failure in Taiwan. *Journal of Hydraulic Engineering*, *138*(2), 186–198. https://doi.org/10.1061/(asce)hy.1943-7900.0000430

Imam, B. M., & Chryssanthopoulos, M. K. (2012). Causes and consequences of metallic bridge failures. *Structural Engineering International: Journal of the International Association for Bridge and Structural Engineering (IABSE)*, *22*(1), 93–98. https://doi.org/10.2749/101686612X13216060213437

Iverson, R. M. (2000). Landslide triggering by rain infiltration. *Water Resources Research*, *36*(7), 1897–1910. https://doi.org/10.1029/2000WR900090

Karlos, V., Solomos, G., & Larcher, M. (2016). *Analysis of blast parameters in the near-field for spherical free-air explosions*.

KAWAI, Y., SIRINGORINGO, D., & FUJINO, Y. (2014). Failure Analysis of the Hanger Clamps of the Kutai-Kartanegara Bridge From the Fracture Mechanics Viewpoint. *Journal of JSCE*, *2*(1), 1–6. https://doi.org/10.2208/journalofjsce.2.1_1

Kim, S., Asce, M., Frangopol, D. M., Asce, D. M., Soliman, M., & Asce, S. M. (2013).

Generalized Probabilistic Framework for Optimum Inspection and Maintenance Planning. *March*, 435–447. https://doi.org/10.1061/(ASCE)ST.1943-541X.0000676.

Kunnath, S. K., Erduran, E., Chai, Y. H., & Yashinsky, M. (2008). Effect of Near-Fault Vertical Ground Motions on Seismic Response of Highway Overcrossings. *Journal of Bridge Engineering*, *13*(3), 282–290. https://doi.org/10.1061/(asce)1084-0702(2008)13:3(282)

Lee, G. C., Mohan, S. B., Huang, C., & Fard, B. N. (2013). *A Study of U . S . Bridge Failures by*.

Limaye, S. V, & Pujari, A. B. (2020). A Review on Progressive Collapse of the Bridge. *International Research Journal of Engineering and Technology*, 3180–3184. www.irjet.net

Lin, C., Han, J., Bennett, C., Parsons, R. L., Deng, L., Wang, W., Yu, Y., Biezma, M. V., Schanack, F., Veletzos, M. J., Restrepo, J. I., Wardhana, K., Hadipriono, F. C., Us, L. E. T., You, R., Kunnath, S. K., Erduran, E., Chai, Y. H., Yashinsky, M., … Setioso, D. C. (2012). Bridge collapses around the world: Causes and mechanisms. *Journal of Performance of Constructed Facilities*, *22*(2), 1–6. https://doi.org/10.5610/jaee.12.4_319

Liu, Y., Ning, B., & Wang, Y. (2012). *Study on Thermal and Structural Behavior of a Cable-Stayed Bridge under Potential Tanker Truck Fires*. *238*, 684–688. https://doi.org/10.4028/www.scientific.net/AMM.238.684

Mitropoulos, P., Abdelhamid, T. S., & Howell, G. A. (2005). Systems Model of Construction Accident Causation. *Journal of Construction Engineering and Management*, *131*(7), 816–825. https://doi.org/10.1061/(asce)0733-9364(2005)131:7(816)

Mohammadi, J., & Polepeddi, R. (2000). *B RIDGE R ATING WITH C ONSIDERATION FOR F ATIGUE*. *August*, 259–265.

NBC News. (2007). *Suicide truck bomb collapses Baghdad bridge.pdf*. https://www.nbcnews.com/id/wbna18033283

Peng, G. (2008). *Effect of thermal shock due to rapid cooling on residual mechanical properties of fiber concrete exposed to high temperatures*. *22*, 948–955. https://doi.org/10.1016/j.conbuildmat.2006.12.002

Priestley, B. M. J. N. (1995). *S e i s m i c s h e a r s t r e n g t h of r e i n f o r c e d concrete*. *120*(8), 2310–2329.

Robertson, I. N., Riggs, H. R., Yim, S. C., & Young, Y. L. (2007). Lessons from Hurricane Katrina Storm Surge on Bridges and Buildings. *Journal of Waterway, Port, Coastal, and Ocean Engineering*, *133*(6), 463–483. https://doi.org/10.1061/(asce)0733-950x(2007)133:6(463)

Scanlan, E.-, Narrows, T., Narrows, O. T., & Creek, L. (1998). *BRIDGE FLUTTER DERIVATIVES AT VORTEX LOCK-IN By Robert H. Scanlan,*. *3*, 450–458.

Son, J., Astaneh-Asl, A., & Rutner, M. (2005). Performance of bridge decks subjected to blast load. *The 6th-Japanese-German-Bridge-Symposium, Munich, Germany*, *29*(1), 9.

Sun, Z., Wang, D., Guo, X., Si, B., & Huo, Y. (2012). Lessons Learned from the Damaged Huilan Interchange in the 2008 Wenchuan Earthquake. *Journal of Bridge Engineering*, *17*(1), 15–24. https://doi.org/10.1061/(asce)be.1943-5592.0000210

Tan, J., Elbaz, K., Wang, Z., & Shen, J. S. (2020). *Lessons Learnt from Bridge Collapse : A View of Sustainable Management*. 1–16.

Taricska, M. (2014). *An analysis of recent bridge failures in the united states*.

Wang, H., Hsieh, S.-C., Lin, C., & Wang, C.-Y. (2014). Forensic Diagnosis on Flood-Induced Bridge Failure. I: Determination of the Possible Causes of Failure. *Journal of Performance of Constructed Facilities*, *28*(1), 76–84. https://doi.org/10.1061/(asce)cf.1943-5509.0000419

Wardhana, K., & Hadipriono, F. C. (2003). Study of Recent Building Failures in the United States. *Journal of Performance of Constructed Facilities*, *17*(3), 151–158. https://doi.org/10.1061/(asce)0887-3828(2003)17:3(151)

Winget, D. G., Marchand, K. A., & Williamson, E. B. (2005). Analysis and Design of Critical Bridges Subjected to Blast Loads. *Journal of Structural Engineering*, *131*(8), 1243–1255. https://doi.org/10.1061/(asce)0733-9445(2005)131:8(1243)

Xu, F. Y., Zhang, M. J., Wang, L., & Zhang, J. R. (2016). Recent Highway Bridge Collapses in China: Review and Discussion. *Journal of Performance of Constructed Facilities*, *30*(5), 04016030. https://doi.org/10.1061/(asce)cf.1943-5509.0000884

Yi, Z., Agrawal, A. K., Ettouney, M., & Alampalli, S. (2013). *Ac N ce ot p C ted op M ye a di nu te s d cr ip t Ac N ce ot p C ted op M ye a di nu te s d cr ip t*. https://doi.org/10.1061/(ASCE)BE.1943-5592.0000547

WEBOGRAPHIE

Why bridges collapse - Google Search. (n.d.). Retrieved March 27, 2022, from https://learnenglish.britishcouncil.org/skills/reading/b2-reading/why-bridges-collapse

Key causes of failure of bridges - Google Search. (n.d.). Retrieved March 27, 2022, from https://civildigital.com/key-causes-failure-bridges-reasons-collapse-during-construction-bridge-failure/#google_vignette

Blast loads - Google Search. (n.d.). Retrieved May 02, 2022, from https://www.sciencedirect.com/topics/earth-and-planetary-sciences/blast-loads

Fiche descriptive de mine - Google Search. (n.d.). Retrieved May 19, 2022, from https://www.google.com/url?sa=t&source=web&rct=j&url=http://bibliomines.org/wp-content/uploads/PPM_2.pdf&ved=2ahUKEwigyOnGj-f4AhXFWMAKHcb7B9wQFnoECAYQAQ&usg=AOvVaw38eHhDeqOE4tMM7De2BadJ

ANNEXES

Annexe A: Tables used in methodology

Terrain category		z_0 m	z_{min} m
0	Sea or coastal area exposed to the open sea	0,003	1
I	Lakes or flat and horizontal area with negligible vegetation and without obstacles	0,01	1
II	Area with low vegetation such as grass and isolated obstacles (trees, buildings) with separations of at least 20 obstacle heights	0,05	2
III	Area with regular cover of vegetation or buildings or with isolated obstacles with separations of maximum 20 obstacle heights (such as villages, suburban terrain, permanent forest)	0,3	5
IV	Area in which at least 15 % of the surface is covered with buildings and their average height exceeds 15 m	1,0	10
NOTE: The terrain categories are illustrated in A.1.			

Table A.1. Terrain categories and terrain parameters

Road restraint system	on one side	on both sides
Open parapet or open safety barrier	d + 0,3 m	d + 0,6 m
Solid parapet or solid safety barrier	$d + d_1$	$d + 2d_1$
Open parapet and open safety barrier	d + 0,6 m	d + 1,2 m

Table A.2. Depth d_{tot} to be used for $A_{ref,x}$

Annexe B: Figures used in methodology

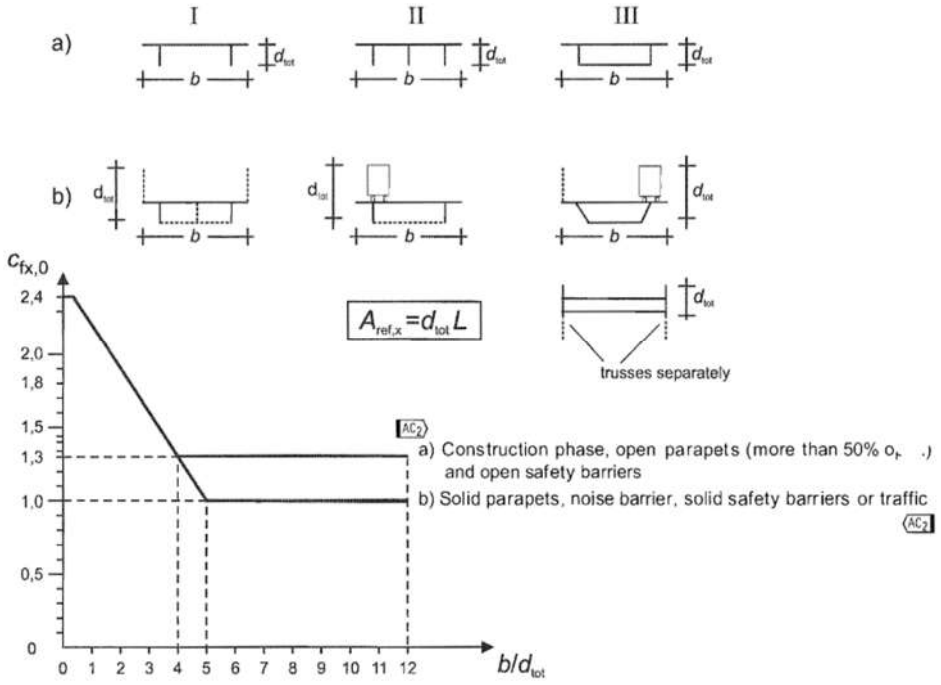

Figure B.1. Force coefficient for bridges, $C_{fx,O}$ (EN 1991-1-4, 2011)

Eurocodes are recent standards covering all of the applications relating to construction. Eurocode 1 is the standard used to determine actions to be carried out on structures (buildings, pylons, towers, etc.). Eurocodes 2 to 9 give the rules for design and for inspection of the resistance and stability of the various types of structures. These standards are consistent with each other, complete, detailed and precise. They apply to all. ***Today, Eurocodes are compulsory.***

Source : Atlas des énergies pour un monde vivable, Syros, 1994.

Cartes des vitesses de vent $V_{b,0}$ [m/s] estimées à partir du potentiel d'énergie éolienne.

$V_{b,0}$ [m/s] wind velocity maps estimated based on the wind turbine energy potential.

L'Eurocode 1 : Actions sur les structures - **Partie 1-4 :** Actions générales - Actions du vent (réf. EN 1991-1-4) défini les paramètres suivants :

L'Eurocode 1 : *Actions on structures - Parts 1-4 : General actions - Wind actions (ref. EN 1991-1-4) defines the following parameters :*

- **$V_{b,0}$:** Valeur de base de la vitesse de référence du vent (vitesse sur 10 minutes à une hauteur de 10m au-dessus du sol en terrain dégagé).
  $V_{b,0}$: *Fundamental basic wind velocity (10 minute mean velocity at a height of 10m above open flat country terrain).*

$V_{b,0}$: Vitesse de référence
$V_{b,0}$: Reference Wind

Zone 1	20 m/s
Zone 2	22 m/s
Zone 3	24 m/s
Zone 4	26 m/s
Zone 5	28 m/s

- **Cr(z)** coefficient de variation de hauteur en fonction de la rugosité du terrain.
  Cr(z) *height variation factor according to the roughness of the terrain.*

Figure B.2. Wind velocity maps estimated based on the wind turbine energy potential.

Annexe C: Figures used in results and interpretation

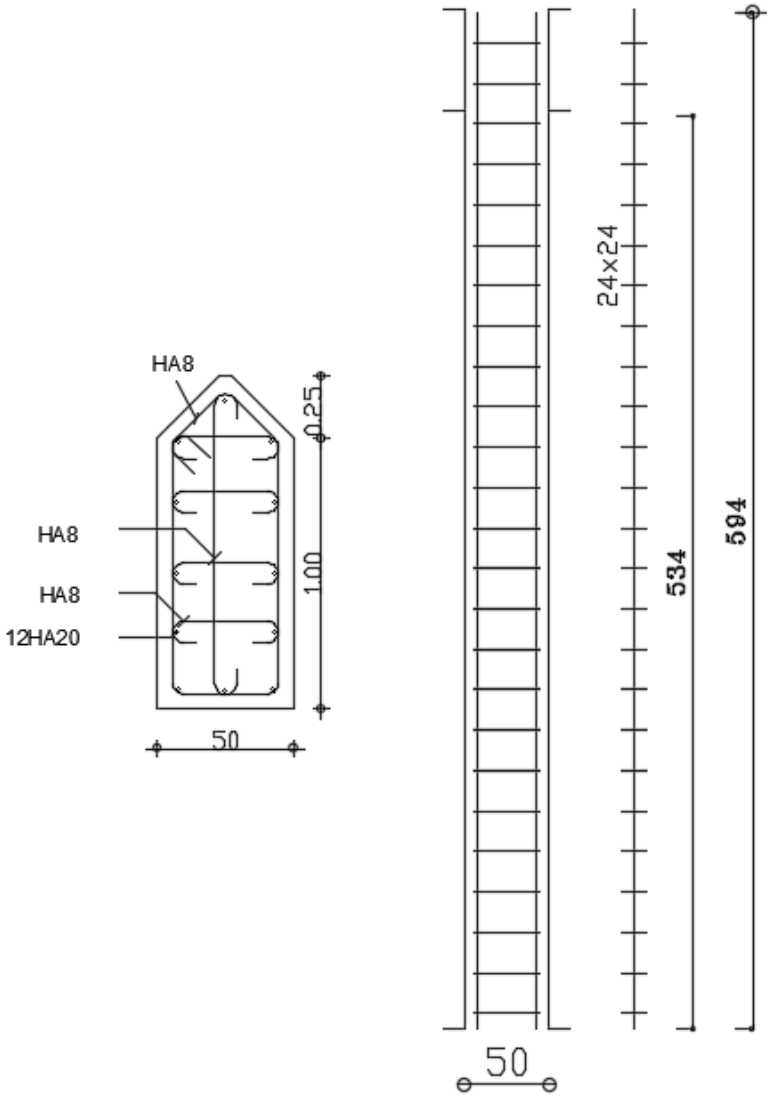

Figure C.1. Reinforcement of pier.

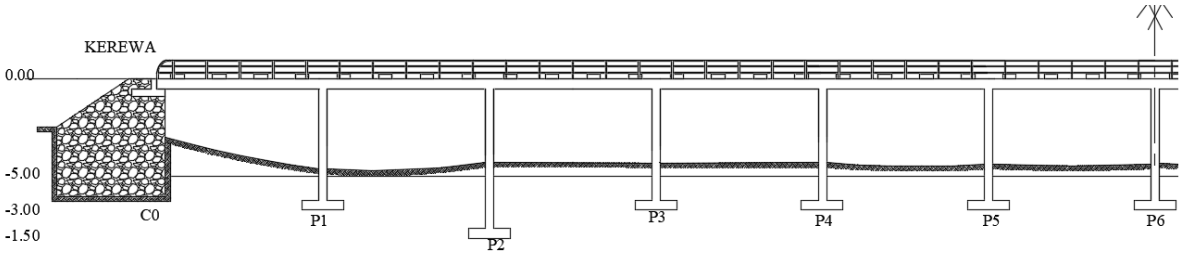

Figure C.2. Longitudinal section of bridge.

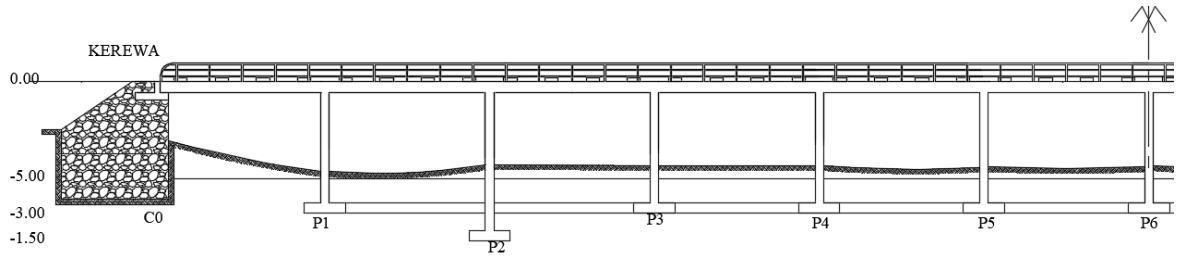

Figure C.3. Longitudinal section of bridge with straightening beam.

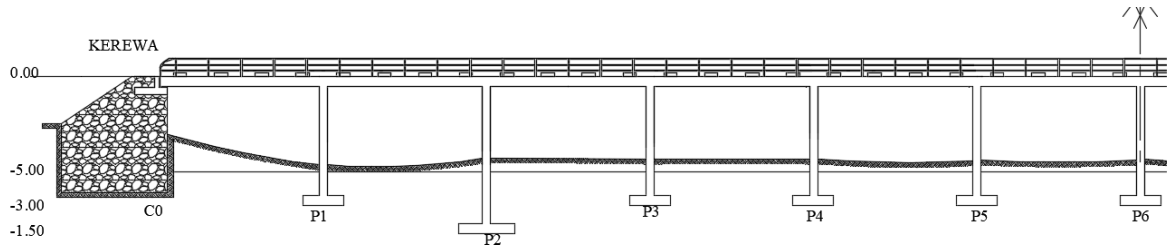

Figure C.2. Longitudinal section of bridge with isolated footing (5 x 3.5) at pier P2.

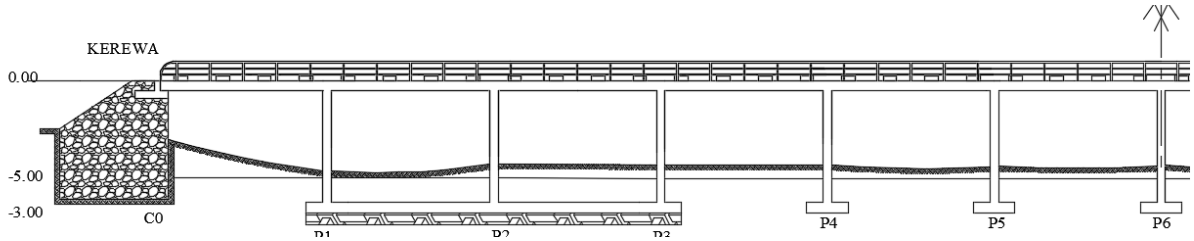

Figure C.2. Longitudinal section of bridge with raft foundation.